

1988

A Kinematical Investigation of Some External Wind Tunnel Force Measurement Systems

Gary A. Peterson

Embry-Riddle Aeronautical University - Daytona Beach

Follow this and additional works at: <https://commons.erau.edu/db-theses>



Part of the [Aerospace Engineering Commons](#)

Scholarly Commons Citation

Peterson, Gary A., "A Kinematical Investigation of Some External Wind Tunnel Force Measurement Systems" (1988). *Theses - Daytona Beach*. 241.

<https://commons.erau.edu/db-theses/241>

This thesis is brought to you for free and open access by Embry-Riddle Aeronautical University – Daytona Beach at ERAU Scholarly Commons. It has been accepted for inclusion in the Theses - Daytona Beach collection by an authorized administrator of ERAU Scholarly Commons. For more information, please contact commons@erau.edu.

A KINEMATICAL INVESTIGATION OF SOME
EXTERNAL WIND TUNNEL FORCE MEASUREMENT SYSTEMS

BY

GARY A. PETERSON

A THESIS PRESENTED IN PARTIAL FULFILLMENT OF
THE REQUIREMENTS FOR THE DEGREE OF

MASTER OF SCIENCE IN AERONAUTICAL ENGINEERING

EMBRY-RIDDLE AERONAUTICAL UNIVERSITY

1988

UMI Number: EP31844

INFORMATION TO USERS

The quality of this reproduction is dependent upon the quality of the copy submitted. Broken or indistinct print, colored or poor quality illustrations and photographs, print bleed-through, substandard margins, and improper alignment can adversely affect reproduction.

In the unlikely event that the author did not send a complete manuscript and there are missing pages, these will be noted. Also, if unauthorized copyright material had to be removed, a note will indicate the deletion.

UMI[®]

UMI Microform EP31844
Copyright 2011 by ProQuest LLC
All rights reserved. This microform edition is protected against
unauthorized copying under Title 17, United States Code.

ProQuest LLC
789 East Eisenhower Parkway
P.O. Box 1346
Ann Arbor, MI 48106-1346

EMBRY-RIDDLE AERONAUTICAL UNIVERSITY

GRADUATE STUDIES

DATE August 1, 1988

I HEREBY RECOMMEND THAT THE THESIS PREPARED UNDER MY

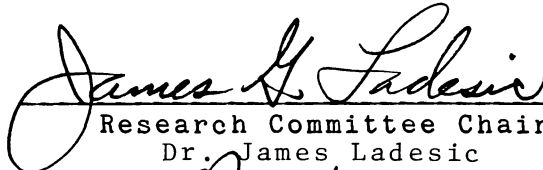
SUPERVISION BY Gary A. Peterson

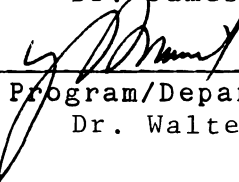
ENTITLED A Kinematical Investigation of Some External Wind

Tunnel Force Measurement Systems

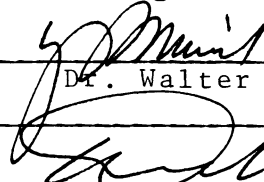
BE ACCEPTED IN PARTIAL FULFILLMENT OF THE REQUIREMENTS FOR

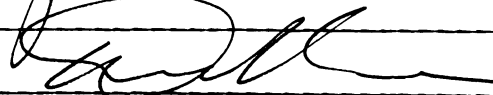
THE DEGREE OF Master of Science in Aeronautical Engineering


Research Committee Chairman
Dr. James Ladesic


Program/Department Chairman
Dr. Walter Schimmel

Recommendation Concurred by Examining Committee:


Dr. Walter Schimmel


Dr. David Kim

ACKNOWLEDGMENTS

The author would like to thank all of the faculty, staff, and students within the engineering department for their many years of support and guidance. A special thanks is extended to committee members Dr. Walter Schimmel and Dr. David Kim for their enthusiastic support of this paper. Finally, the author thanks Dr. James Ladesic who, as committee chairman, sacrificed many hours of personal time on behalf of this thesis. Without the guidance and counsel of Dr. Ladesic, little of this work would have been possible.

TABLE OF CONTENTS

LIST OF ILLUSTRATIONS v

NOMENCLATURE viii

ABSTRACT x

Chapter

I. INTRODUCTION 1

 A. Historical Development 2

II. BACKGROUND 7

 A. Wind Tunnel Balances 7

 B. Basic Concepts 12

III. PYRAMIDAL FORCE BALANCE 18

 A. Concept 18

 B. Static Analysis 25

 C. Uncertainty Analysis 45

IV. OTHER FORCE BALANCES 58

 A. Six Component Floating Beam 58

 1. Concept 58

 2. Static Analysis 63

 B. Three Component Strain Gaged Strut 68

 1. Concept 68

 2. Static Analysis 69

 3. Uncertainty Analysis 70

V. CLASSIFICATION OF FORCE BALANCES 74

 A. Classification Method 74

 B. Outline of Method 77

Chapter

VI. CONCLUSIONS	80
A. General	80
B. Balance Systems	81
C. Classification	82
D. Recommendations	84
APPENDIX A	
Numerical Uncertainty Example: Pyramidal Balance	86
APPENDIX B	
Numerical Uncertainty Example: Strain Gaged Strut	88
APPENDIX C	
Classification Examples:	
A. Two Component Strain Gaged Strut	89
B. Three Component Strain Gaged Strut	92
C. Six Component Floating Beam Balance	93
D. Three Component Pyramidal Balance	96
E. Six Component Pyramidal Balance	97
F. Three Component Smoke Tunnel Balance	100
G. Six Component Platform Balance	104
H. Six Component Yoke Balance	107
BIBLIOGRAPHY	110

LIST OF ILLUSTRATIONS

Figure	Page
1. Typical internal/sting balance configuration. ...	7
2. Typical external/strut balance configuration. ...	8
3. The "Balance" concept.	11
4. Frame with load L.	13
5. Frame with load D.	13
6. Frame with load M.	14
7. Frame with load cells a, b, and c.	14
8. Loaded frame with load cells a, b, and c.	15
9. Modified frame with lift load L.	19
10. Modified frame with drag load D.	19
11. Modified frame with moment load M_p	20
12. Frame with lower linkage and a lift load, L.	20
13. Frame with lower linkage and a drag load, D.	21
14. Three component pyramidal balance configuration.	22
15. Six component pyramidal balance configuration. ..	23
16. Pyramidal balance components.	25
17. Platform free body diagram: three component.	26
18. Main frame free body diagram: three component. ..	27
19. Lower lever system: three component.	28
20. Pyramidal link dimensions: six component.	29
21. Platform free body diagram: six component.	30
22. Balance dimension relationships.	32
23. Platform free body diagram: x-y plane.	33

Figure	Page
24. Platform free body diagram: y-z plane.	34
25. Platform free body diagram: x-z plane.	35
26. Symmetric force components on platform.	35
27. Main frame free body diagram: six component.	38
28. Main frame free body diagram: x-y plane.	40
29. Main frame free body diagram: y-z plane.	40
30. Symmetric force components on main frame.	41
31. Lower lever system: six component.	42
32. Lower lever system: symmetric half in x-y plane.	43
33. Lower lever system: symmetric half in x-y plane.	43
34. Drag/Yaw frame: six component.	44
35. Uncertainty diagram	45
36. % From Nominal versus Case histogram: pyramidal.	55
37. Floating beam balance configuration.	59
38. Floating beam free body diagram.	64
39. Yaw flexural element.	67
40. Three component strain gaged strut configuration.	68
41. % From Nominal versus Case histogram: strut.	72
42. Two component strain gaged strut.	89
43. Lift applied to two component strut.	91
44. Drag applied to two component strut.	91
45. Six component floating beam hardware tolerance locations.	95

Figure	Page
46. Three component pyramid hardware tolerance locations.	96
47. Six component pyramid hardware tolerance locations.	98
48. Three component smoke tunnel balance configuration.	100
49. Smoke tunnel balance deflections.	101
50. Free body diagram of smoke tunnel balance element c.	102
51. Smoke tunnel balance hardware tolerance locations.	103
52. Six component platform configuration.	104
53. Platform balance hardware tolerance locations. ..	106
54. Six component yoke configuration.	107
55. Yoke balance hardware tolerance locations.	108

NOMENCLATURE

a	load cell, assembled dimension in pyramid
A	cross sectional area
b	load cell, pyramidal platform half-width
B_1, B_2	partial lift reactions in lever system
c	load cell, machined dimension on pyramid main frame, coupling number
c'	yaw reaction dimension in pyramid
D	drag force
d	pyramid link length
D_{y1}, D_{y2}, D_{x1}	drag reactions
e	machined dimension on pyramid platform
f	lower lever system dimension, drag/yaw frame dimension on pyramid
F_1, F_2, F_3, F_4	lower link reactions on main frame
F_L	lift force reaction on pyramid
F_D	drag force reaction on pyramid
h	pyramid link height
k	machined dimension on pyramid platform
L	lift force
L_{y1}, L_{y2}	lift reactions
m	pyramid main frame dimension
M_p	pitch moment
M_R	roll moment
M_Y	yaw moment

n	degree of coupling
N	side force reaction on pyramid
P	pitch moment reaction on pyramid
p	hardware parameter
Q ₁ , Q ₂	drag/yaw reactions on pyramid main frame
R ₁ , R ₂ R ₃ , R ₄	moment reactions, axial forces in pyramidal links, floating beam reactions
R	roll moment reaction on pyramid
R _L	lift force reaction on pyramid
R _D	drag force reaction on pyramid
R _x , R _y , R _z	components of axial link forces
S	side force
w _a , w _b , w _c , w _c , w _d , w _e , w _h , w _k	dimensional uncertainties
w _{R1} , w _{R2} , w _{R3} , w _{R4}	uncertainties in the pyramidal link axial loads
w _P , w _R , w _Y , w _{FL} , w _{FD} , w _N	uncertainties in the pitch, roll, yaw, lift, drag, and side force reactions, respectively
x, y, z	coordinate axis
Y	yaw moment reaction on pyramid

ABSTRACT

A discussion on the fundamental concepts associated with wind tunnel forces measurement systems (balances) is presented. Detailed static analyses are performed on the six component pyramidal, six component floating beam, and three component strain gaged strut balances. These static analyses lead to a dimensional uncertainty investigation of the pyramidal and strain gaged strut balances. The critical dimensions for the pyramidal balance are found to be the lengths of the pyramidal links, the platform half-width, and the model attachment strut. No single dimension on the strain gaged strut is more critical than the others.

A new method for the classification of wind tunnel force balances is presented. This method uses two defined quantities: the degree of coupling, and a hardware parameter based on the number of areas where tolerances are of a concern. The versatility of the method is demonstrated through a number of classification examples.

The following recommendations are made: determine the effects of component deflection on the pyramidal force balance readouts and investigate the uncertainties associated with low strains on the three component strain gaged strut.

To Mom, Dad, and Laurie, my beautiful sister.

CHAPTER I
INTRODUCTION

Historically, there has been a need for a dependable and effective means of measuring and predicting the aerodynamic characteristics of an arbitrarily shaped body immersed in a flowing fluid. To date, the most important devices used to meet this need have been wind tunnels and their force balances. There are many advantages to using scaled or even full size models; the most notable being cost and safety. Economically, initial wind tunnel testing of a design is more efficient than blindly developing and building a full size prototype. Furthermore, the flight characteristics of a vehicle can be determined with a high degree of certainty, thereby reducing the hazards associated with flight testing. The greatest setback to such testing is the lack of similitude. For the incompressible fully immersed flow condition, the test data is valid only when the Reynolds number (ratio of the inertial to viscous forces) closely matches that of the full scale case. It is here that many of the pitfalls of wind tunnel testing are encountered. These similitude difficulties were not fully understood by the early pioneers of aviation. Therefore, they are largely responsible for the lack of any significant advances in aerodynamic testing during the centuries leading up to the Wright brothers' first flight.

A. Historical Development:

Of the earliest aeronautical dreamers, Leonardo da Vinci was perhaps the most well known [1,2].* At his death in 1519, he left some 150 sketches of flying machines. His concepts and those of many inventors during this early era were based upon imitating the flapping motion of birds with devices called ornithopters. As the next few centuries passed, few technological advancements were made with heavier than air flight vehicles. The first person to set forth the concept of fixed wing flight was George Cayley of England [1]. In 1799 he proposed separating the lift requirements of an airplane from its propulsion requirements. The next several years were marked by tremendous conceptual development by Cayley until in 1804 he designed and built a model glider. This glider represented the first modern configuration airplane in history. In 1853, Cayley was also responsible for the first human carrying glider. Little is known about its design or the date on which it flew, but it is said to have carried Cayley's coachman several hundred yards.

During the mid to late nineteenth century, a number of other aviation pioneers experimented with and flew gliders. The most significant of them was Otto Lilienthal of Germany [1,2]. Lilienthal built a number of gliders and flew over 2,500 successful flights. Had he not been killed in a freak glider accident in 1896, many believe that Lilienthal would have achieved powered flight before the Wright brothers.

* Bracketed references are listed on page 110.

Other inventors who experimented with gliders and powered machines included Percy Pilcher, Octave Chanute, and Samuel Langley. Pilcher was a student of Lilienthal and continued on with much of his glider work. In 1899, he also died in a glider crash, and like Lilienthal, many believe Pilcher could have been the first man to attain powered flight. Octave Chanute was one of the first Americans to seriously consider mechanical flight. In 1894, he published the book Progress in Flying Machines; a classic piece of literature that sparked much of the Wright brothers' interest in flying. Consequently, Chanute became a close friend of the Wright brothers and played an important role in the design of their flying machines. Samuel Langley, secretary of the Smithsonian Institute, developed and attempted to fly a powered machine during the same period of time as the Wright brothers. His machine, known as the Aerodrome, failed in two attempts to be catapulted off of a houseboat just nine days prior to the Wright brothers first successful flight. Finally, there are the Wright brothers themselves. Little needs to be said about these two men because their vigorous and scientific approach to the research and development of their ideas are well known to all.

Each of the above mentioned pioneers made immeasurable contributions to the aeronautical sciences. Unfortunately, due to their lack of knowledge about the "elusive" aerodynamic forces, they were unable to quantitatively evaluate scaled versions of their many imaginative designs

and ideas. As a result, these early inventors had no choice but to test, over and over, full size prototypes in a vain attempt to make these designs fly. In fact, today there remain a number of aspects of aerodynamics that can still be considered elusive.

The first truly meaningful attempt at experimentally measuring aerodynamic forces was done in 1804 by Cayley [1]. Cayley developed a rotating arm apparatus on which a lifting surface could be mounted. From this, he crudely estimated the aerodynamic forces and center of pressure acting on airfoils. The downfall of this concept was that after a few rotations, the air in the vicinity of the arm would also begin to rotate. Still, this was an important first step in aerodynamic testing.

In 1871, the first known wind tunnel was built in England by Francis Wenham [1,3]. By today's standards, this tunnel was very crude and lacked the aerodynamic control of flow turbulence and steadiness. Yet, Wenham was still able to measure the lift and drag on models with a balance type arrangement consisting of weighing beams. The weighing beam concept, or "balance", will be described in Chapter II in more detail. After Wenham, a number of researchers built wind tunnels and conducted a wide range of tests. Men such as Horatio Phillips, Nikolai Joukowski, Dr. Ludwig Mach, and Dr. A. Heber Zahm all conducted various research activities with their own wind tunnels.

Finally, in 1901, the Wright brothers designed and built their own wind tunnel [1,3]. With this wind tunnel,

Orville and Wilbur were able to make the first systematic series of wind tunnel tests on airfoil sections. To accomplish this, they had to design and build their own force measurement system from which they measured the lift to drag ratios applied to the test shapes. The system that they used actually consisted of two devices [4]. One would measure only the lift force acting on an airfoil shape and the second would read the lift to drag ratio. The lift apparatus measured the lift in terms of the drag on a flat plate. The mechanism was designed so that the drag force of the plate would be counterbalanced (through a set of levers) by the lift on the airfoil. By knowing the drag force, measuring the deflection of the levers, and using simple statics, the lift of the surface could be found. The Wrights also noted what they considered to be errors in the data, especially those due to interference effects. The results of their tests in 1901 laid the groundwork for their first successful flight in 1903.

After the Wright brothers' research, many more wind tunnels were built [3]. Most noteworthy were those built by pioneers such as Ludwig Prandtl and Gustav Eiffel. Prandtl's wind tunnel was completed in 1908 and was the first to feature a closed circuit with return air. Eiffel's wind tunnel was built in 1909 and featured a circular cross section. As more and more testing was being done in wind tunnels, the need was set for a device to accurately measure the aerodynamically applied forces and moments on a test

model. The use of data acquired by wind tunnel tests served to establish what today is considered a routine practice. Credible data measured in controlled tests served the Wright brothers in their design efforts just as they do engineers in today's modern aircraft industry. However, there has been an immense change in the sophistication and means by which data is acquired.

CHAPTER II

BACKGROUND

A. Wind Tunnel Balances:

Since the Wright brothers' experiments, a large number of designs and configurations for wind tunnel force measurement systems, or balances, have been developed. Most sources agree that wind tunnel balances can be divided into two broad categories: internal and external [5,6]. Figures 1 and 2 illustrate the internal/sting and the external/strut configurations, respectively. A "sting" is best defined as a balance support that exits the aft end of the model. Likewise, a "strut" can be characterized as a

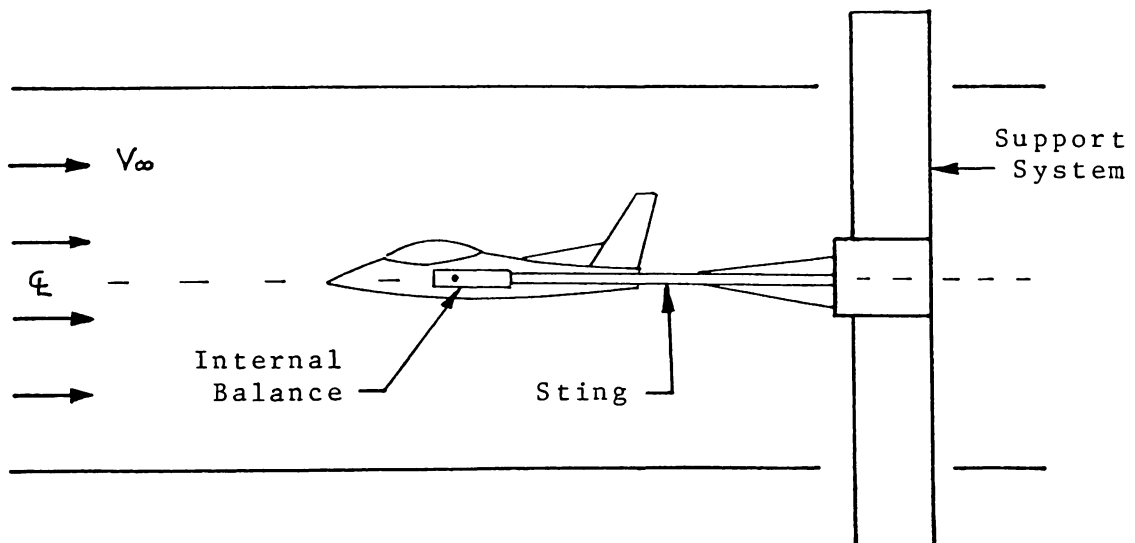


Fig. 1. Typical internal/sting balance configuration.

support that is attached to a point on the model where the forces and moments are to be resolved.

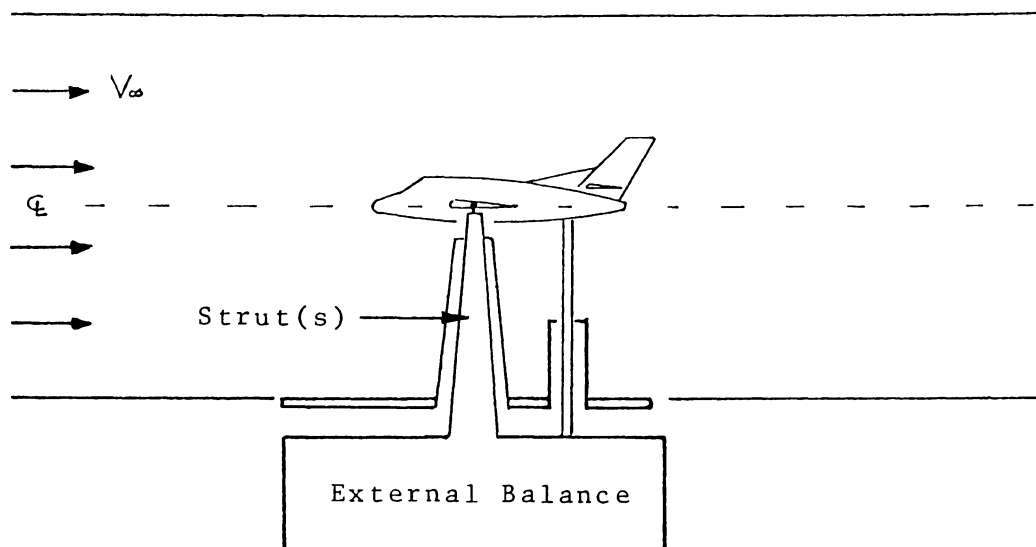


Fig. 2. Typical external/strut balance configuration.

Internal balances are those in which the forces are measured by a device that is generally located within the model itself. An internal balance is often associated with a sting type configuration where the balance support, wires, and any other hardware exit the aft end of the model downstream of the test section, (Figure 1). Generally, the sting type mount combined with an internal balance is commonly used in transonic (Mach numbers from about 0.7 to 1.3), supersonic (Mach numbers from 1.3 to 5.0) or any high Reynolds number tests. The main advantage of the sting/internal balance is the reduction of interference effects that occur with strut type mounting systems. A disadvantage of internal balances is that they are often small and delicate, and functionally depend upon precise, close tolerance machining.

Figure 2 shows the second category of balances. These are external type balances. An external balance is outside the model and the wind tunnel test section. Therefore, the forces and moments are transmitted from inside the test section to the measuring system and quantified accordingly. This is usually accomplished by a series of mechanical linkages and fittings that have been machined to very close tolerances. The most common type of mount associated with the external balance is a simple strut. However, it is entirely possible to have a model mounted on a sting/external balance combination. This thesis will concentrate predominantly on external balances with some reference to internal balances when warranted.

Considering the remarkable advances that have been made in the aerospace field during the last ninety years, there have been relatively few major revisions in wind tunnel balance designs. Many of the early designs were arranged in such a way that the model was mounted on either a vertical post or suspended from a set of wires. At that time, the vertical post was a very popular method of mounting models. In 1925, the suggestion was made by Jean Kerneis [7] that wire suspension would be a superior way to mount a model for testing. It was reasoned that the wires would not produce as great an aerodynamic interaction between the model and its supports. It was also recognized at the time that the wires had the distinct disadvantages of high aerodynamic drag and low suspension system rigidity. This lack of

rigidity can give rise to several difficulties, primarily with the incident angles of the model to the air flow. As the velocity of the air in the test section is increased, a system with low rigidity will allow the model to deflect and change its angles of pitch, yaw, and roll. Unless the system used to measure these angles is held independent of the deflection, erroneous data will be recorded. Furthermore, the combined effect of low rigidity and vortex shedding from the wires can lead to undesired dynamic phenomena such as flutter. Finally, most force measuring systems will suffer a deterioration in their ability to separate the forces when excessive deflections are allowed. It is interesting to note that many of the original balance systems utilized rigid model supports; then for many years the wire suspension method was very popular. Now, due to a better understanding of aerodynamic interactions and a greater desire for smaller system deflections, rigid model supports are again used almost exclusively for most conventional testing.

The term "balance" was coined by the configuration of the early force measuring devices (Figure 3). For many years, an elaborate system of weights, chains, and electrical contacts was used to determine the forces acting on a model [6,8]. In essence, these forces were transmitted through the mounting system to the exterior of the tunnel and into the balance. Each force would then be resolved in such a manner so as to act on a lever which, in turn, would cause the lever to deflect about its fulcrum. On the

opposite side of this lever would be the counterbalance mechanism, usually consisting of a motor and a sliding weight. As the lever would deflect in either direction, electrical contacts would cause the motor to slide the weight; thus restoring the lever to its original "balanced" condition.

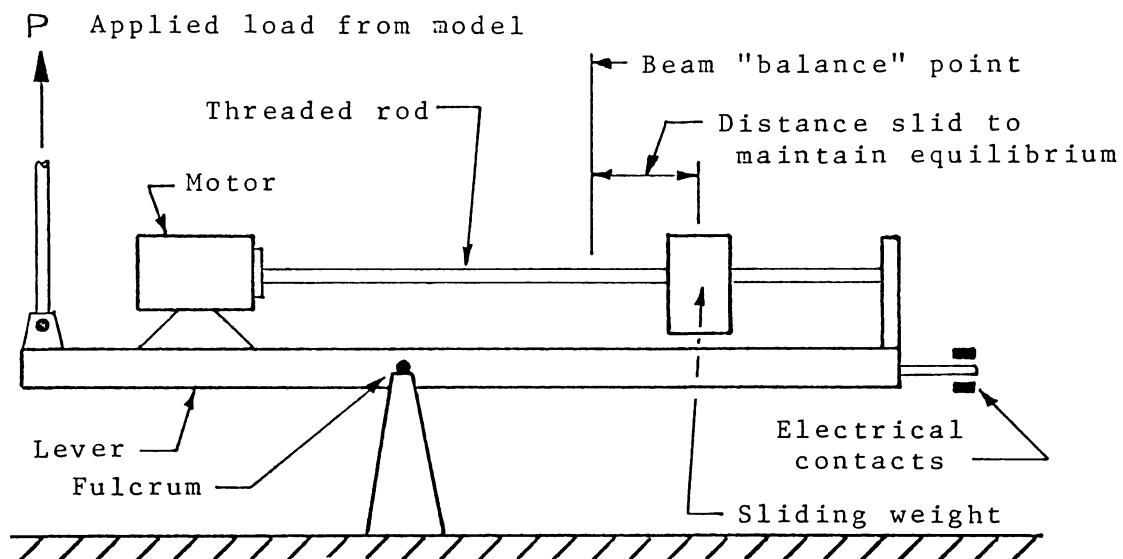


Fig. 3. The "Balance" concept.

The magnitude of the force acting on that segment of the system could then be determined from the required distance that the weight was slid to maintain equilibrium.

To date, the single most significant advancement in wind tunnel force balance technology has been made possible by the advent of electrical strain gages. With the use of strain gages, balances can be made more rigid and durable since the aerodynamic loads are measured directly from the flexure of a spring element. This has eliminated much of

the error prone linkage. In effect, strain gages have eliminated the previously described "balance" concept from force measuring systems. In the 1940's and 1950's, the application of strain gages became widespread in nearly all wind tunnel force balance systems. To this day, they are still the foundation for nearly all of the load cells within a balance.

As for the future, the next generation of wind tunnel balances will likely utilize the concept of magnetic suspension. The foremost advantage of this concept is that no supports or struts are physically attached to the model, thereby eliminating the interference effect that plagues all current model testing. Design and cost studies are presently being done by NASA Langley to evaluate the feasibility of this technology [9]. NASA has a thirteen inch magnetic suspension wind tunnel upon which microprocessor and inertial guidance research is being conducted. However, it should be noted that this technology is still a long way from practical implementation. Consequently, the present designs employing strain gage systems will still be in use for many years to come.

B. Basic Concepts:

The following discussion is a review of the fundamental concepts associated with wind tunnel balance design.

First, consider only a simple, two dimension, triangular frame with a vertical force (L) applied to its vertex as shown in Figure 4.

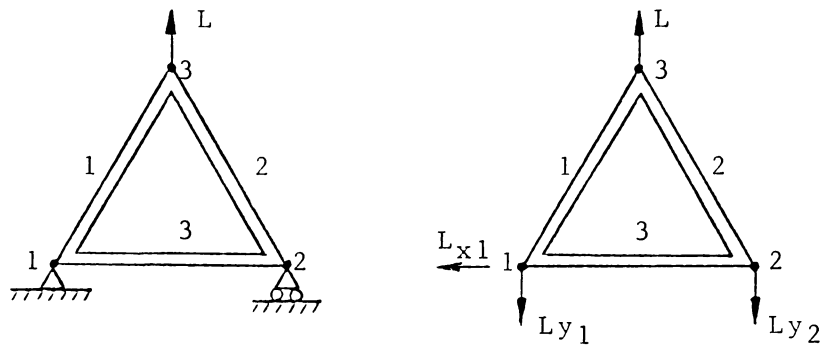


Fig. 4. Frame with load L.

By inspection, the following may be concluded from Figure 4:

1. In the free body diagram, reactions are given as L_{x1} , L_{y1} & L_{y2} . L_{x1} is equal to zero.
2. Assuming no deflections, elements 1 and 2 will be two force members with only axial loads (i.e., no bending moments are induced on any element of the system).

Thus, if L_{y1} and L_{y2} are measured, L is found by the equation:

$$L = L_{y1} + L_{y2}$$

With a horizontal load (D) applied at this same node, the diagram appears as follows:

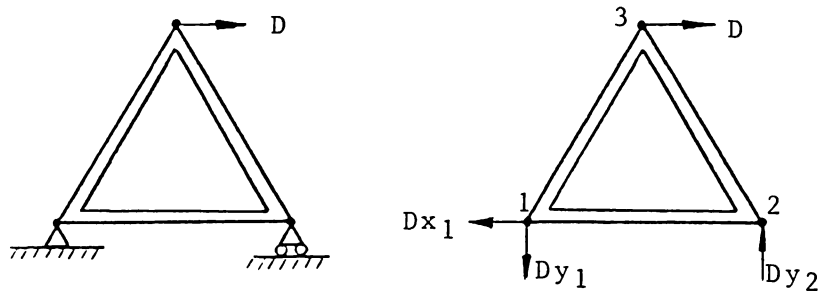


Fig. 5. Frame with load D.

Again, the same comments apply here as for the vertical load L. In this case, D can be found directly by measuring D_{x1} .

Now, suppose a moment is placed at node 3:

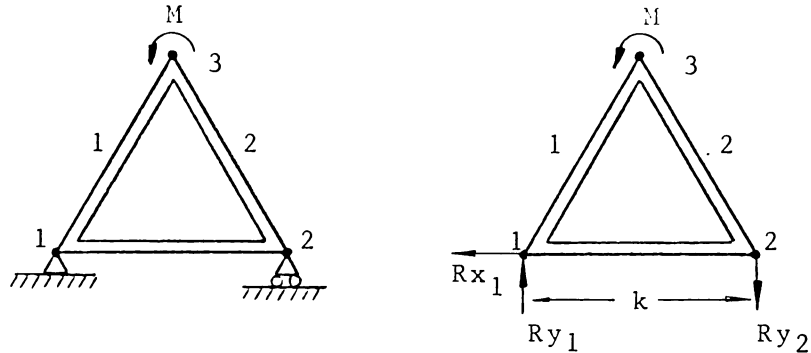


Fig. 6. Frame with load M.

By measuring R_{y1} and R_{y2} in Figure 6, M can be found by:

$$M = (R_{y1} + R_{y2})(k / 2)$$

It is important to note that in this case, because this is a frame structure, elements 1 and 2 are no longer free of bending moments as they were with the applied loads L and D. This is the foundation upon which the pyramidal balance concept is built.

A simple force balance is then obtained by connecting load cells at nodes 1 and 2 to measure the reactions at these points:

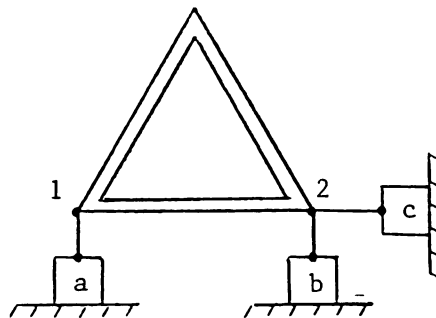



Fig. 7. Frame with load cells a, b, and c.

Items (a), (b), and (c) in Figure 7 may be common load cells such as spring scales, flexural elements affixed with strain gages, commercially purchased load cells, or any other practical devices with which to measure forces.

In Figure 7, linkage is shown connecting the triangular frame structure to the load cells. The notation  symbolizes a rod element with a ball joint or pinned ends. Transverse loads are not reacted by the links. Thus, these links act as filters to assure that the horizontal and vertical components of the support reactions are as decoupled as practicable before the measurement is made.

When any single force or moment is applied to this system, its magnitude can be determined by the load cells and the geometry of the system as previously outlined. When a combination of loads is applied, as shown in Figure 8, the task of determining the magnitude of each force and moment becomes more involved.

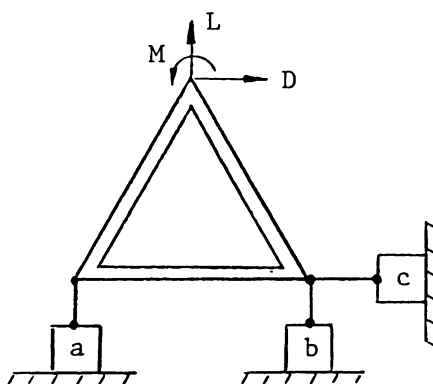


Fig. 8. Loaded frame with load cells a, b, and c.

In this instance, the readout of load cell (a), as with load cell (b), will be a combination of the reactions due to

loads L, D, and M. Only cell (c) is still able to directly read a force, namely D. Therefore, load cells (a) and (b) are both coupled, meaning that their readings must now be substituted into a set of relations that are derived based on the balance's geometry and connectivity of various parts. By this definition, cell (c) is uncoupled for the load D. The proof will be shown in Chapter III.

A number of compromises can be seen between coupled and uncoupled force measuring systems. Generally, simpler mechanical systems will exhibit higher degrees of coupling between their readout channels. Coupled readings have the difficulty of having to rely more on calibration to establish a set of coefficients for the simultaneously solved equations. This is true because the level of confidence in a coupled balance will tend to be lower than that of an uncoupled system. Consequently, a coupled balance may require more calibrations which would increase the amount time needed to test. When a balance design attempts to decouple the load readouts, the mechanical linkage required is often very complex. If there is any clearance, missalignment, or excessive deflection in the linkage system, large errors will be incurred in the readouts.

With most balance designs, it is preferable to attempt to overcome the mechanical tolerance and deflection problems associated with linkages and decouple the forces as much as possible. This is especially true with external balances

because of the amount of available space in which to place the balance equipment. Internal balances, on the other hand, are often highly coupled due to their inherent small size limited by the internal volume within a model.

There are two ways in which balances can be evaluated; each as important and necessary as the other. One is an analytical study where the kinematics, statics, uncertainties, and deflections of the balance design are studied to determine their effect on the output. The other is the calibration process. Ultimately, the determination of the balance's coupling and load reading capabilities are found through calibration. It may be argued that if the final load data is determined by calibration data, why bother with an extensive analytical study? The reasons are as follows. An analytical investigation is needed to determine the critical dimensions that will give low uncertainties and deflections (areas of high stress), to identify possible balance non-linearities, and for a general understanding of the system. It is also helpful in determining the extent to which coupling exists; thus offering some guidance to the calibration process.

CHAPTER III
PYRAMIDAL FORCE BALANCE

A. Concept:

Three Component:

The first configuration to be considered is the three component pyramidal force balance. Understanding the basic three component balance will help in the understanding of the six component arrangement.

Expanding upon the basic frame outlined by Figure 8 in Chapter II, the applied forces are:

L - lift
D - drag
 M_p - pitching moment

Considering only the lift load, as in Figure 4, a few alterations must be made to the frame structure. For the pyramidal balance, node 3 is considered to be the point of resolution where all of the forces and moments are applied. Due to interference effects, it would be impractical to have elements 1 and 2 extend up into the tunnel airstream. As a result, they are terminated just below the tunnel floor and connected to a strut. This transforms the triangular frame into a mechanism capable of motion (Figure 9).

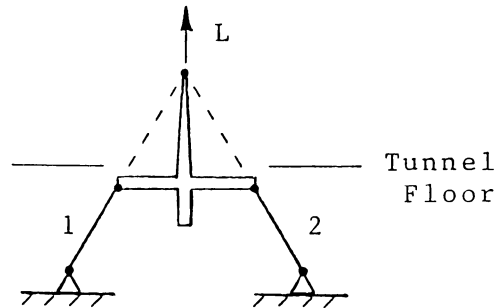


Fig. 9. Modified frame with lift load L .

It is important to note that the projection of elements 1 and 2 continue to pass through the point of resolution (node 3). Because of this, the statics of this new configuration for lift loads remains exactly the same as before.

The same also holds true for just a drag load (Figure 10).

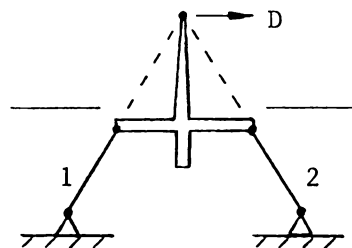


Fig. 10. Modified frame with drag load D .

As long as elements 1 and 2 are aligned with the point of resolution, they will react axially and the mechanism will not collapse.

However, the case of the applied pitching moment is different. Here, an extra reaction, R , is needed to prevent the mechanism from collapsing (Figure 11).

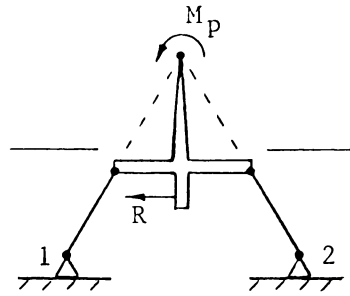


Fig. 11. Modified frame with moment load M_p .

This reaction is present and necessary for an applied moment but is not present for the lift or drag loads.

Thus far, the reactions at the bottom of the structure have been ignored. If load cells were simply placed at nodes 1 and 2, then the same coupling problems would be encountered as discussed in Chapter II. To avoid this, a set of linkages is commonly used (Figure 12).

Again, consider only a lift load on the modified mechanism:

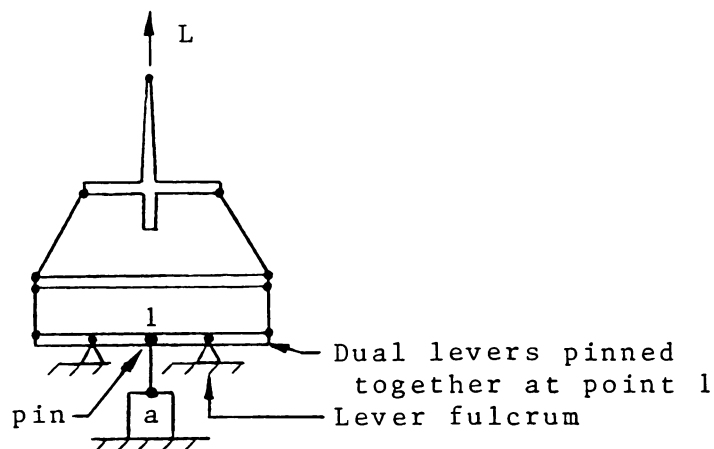


Fig. 12. Frame with lower linkage and a lift load, L .

With the configuration of Figure 12, load cell (a) will register only the lift load L as will be shown later in Section C of this chapter.

With a drag load cell added to the system, the resulting configuration is shown in Figure 13:

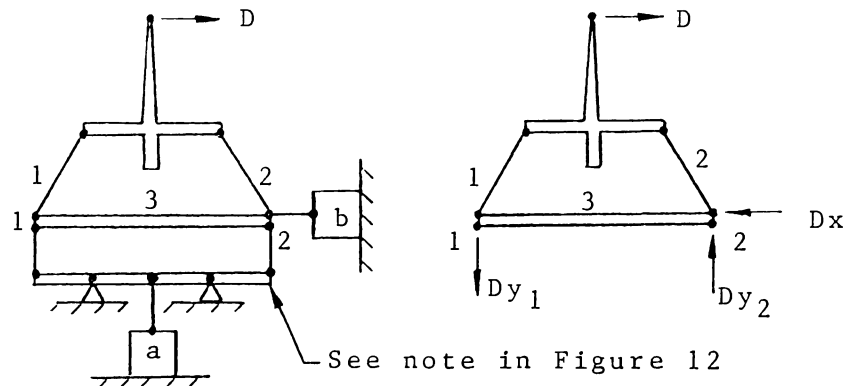


Fig. 13. Frame with lower linkage and a drag load, D .

It is seen in Figure 13 that vertical reactions D_{y1} and D_{y2} cancel each other through the linkage system. Therefore, the lift load cell, (a), is not affected by the drag load. Load cell (b) will thus read the drag, D , directly.

To read a moment, a third load cell, (c), is added to the reaction point previously discussed. To accomplish this, an outer frame is used, in effect replacing element 3 shown above. The moment load cell can not be simply mounted to "ground" since this would create another reaction acting on the system (Figure 14). The final three component balance configuration thus appears as:

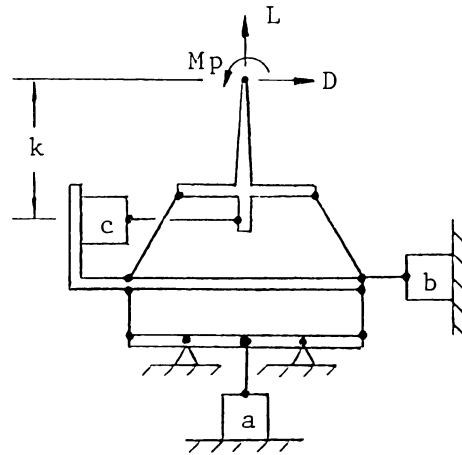


Fig. 14. Three component pyramidal balance configuration.

The moment, M_p , is found by simply multiplying the load on cell (c) by the length (k).

With this setup, all of the loads are separated and no coupling occurs. This fact will be proven in Section C of this chapter. In reality, some coupling will occur regardless of what the static analysis shows due to the elastic deflections and geometric displacements from the numerous parts that compose the balance. These changes in geometry and their associated coupling effects are present in all force balances and are the reason why calibration is always necessary. As mentioned earlier, this system is mechanically more complex than it would be if the full magnitude of coupling were allowed.

Six Component:

With only minor modifications, the same concepts used with the three component design are used with the six component configuration (Figure 15). The fundamental difference is in the manner in which the yawing moment is decoupled. Note that the components of lift, side force,

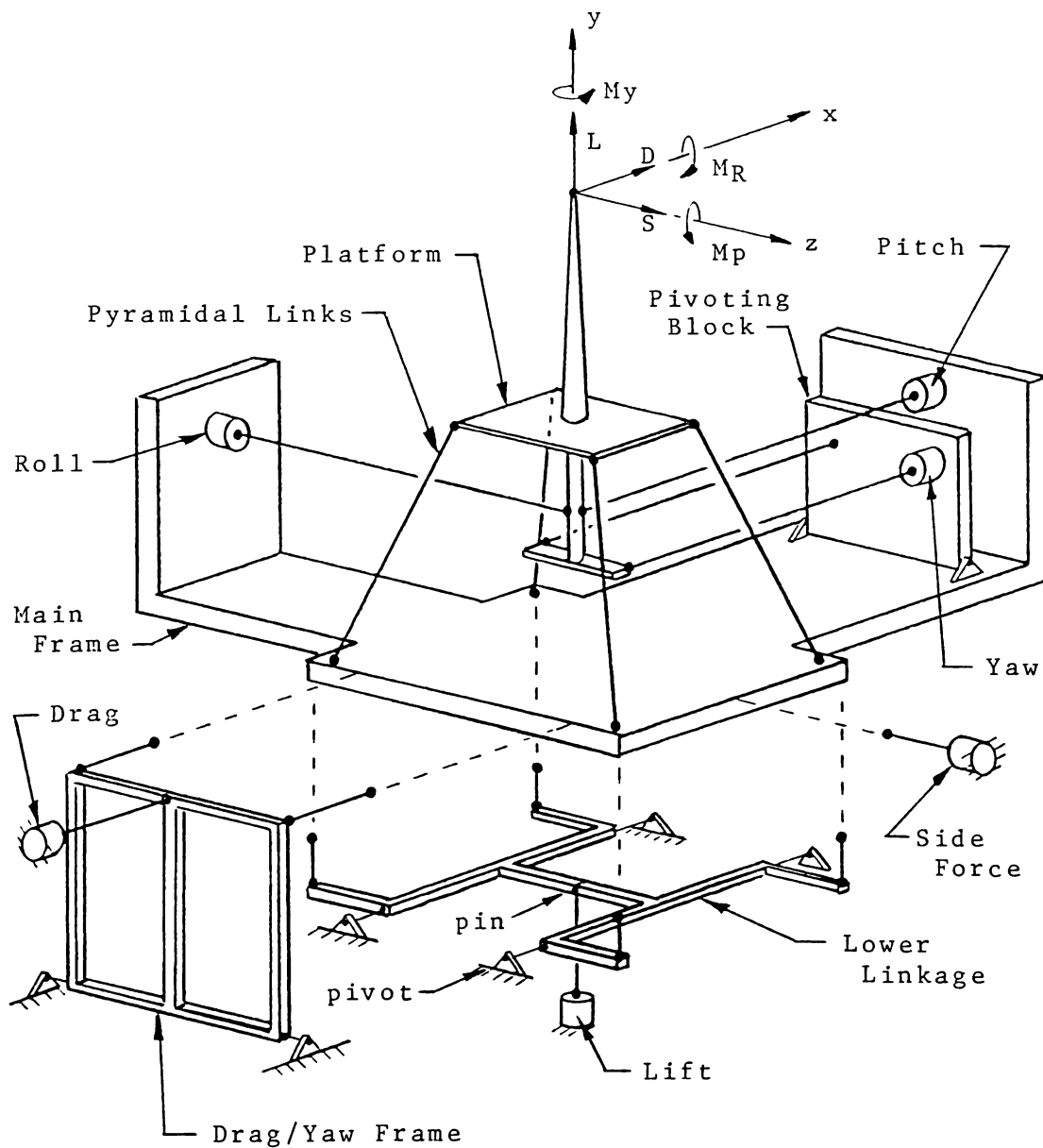


Fig. 15. Six component pyramidal balance configuration.

and rolling moment are separated just like the three component balance previously discussed.

As mentioned earlier, a hardware modification must be made to accommodate the yawing moment. Looking downward on the main frame, it is seen that the yaw load cell is mounted on a stiff pivoting block. This block, as shown in Figure 15, will not deflect under a yawing moment but will pivot slightly when a pitching moment is applied. Thus, the yaw load cell is separated from the pitching moment. Furthermore, the yawing moment will tend to rotate the entire main frame. To counter this, a double set of links are attached to the outside of a pivoting drag/yaw frame. The drag load cell is then connected to the center of the frame. Under a yawing load, the main frame is held in place by the outer links on the drag/yaw frame. This places the drag/yaw frame into torsion and no load is directed to the drag load cell. On the other hand, a drag force will load the outer links in the same direction, causing the drag/yaw frame to pivot slightly about its support. The drag load cell is then uncoupled from the yawing moment and will measure only the applied drag force.

B. Static Analysis:

The pyramidal balance can be divided into three basic sub-systems, all of which are interconnected by linkages (Figure 16):

1. Platform: Contains the strut and distributes the forces to the pyramidal links.
2. Main frame: Component on which all of the moment load cells are mounted. It distributes the loads to the force load cells and the lever system.
3. Lever system: Separates the drag, side, pitch, and roll reactions from the lift load cell.

These three sub-systems are common to both the three and six component balances.

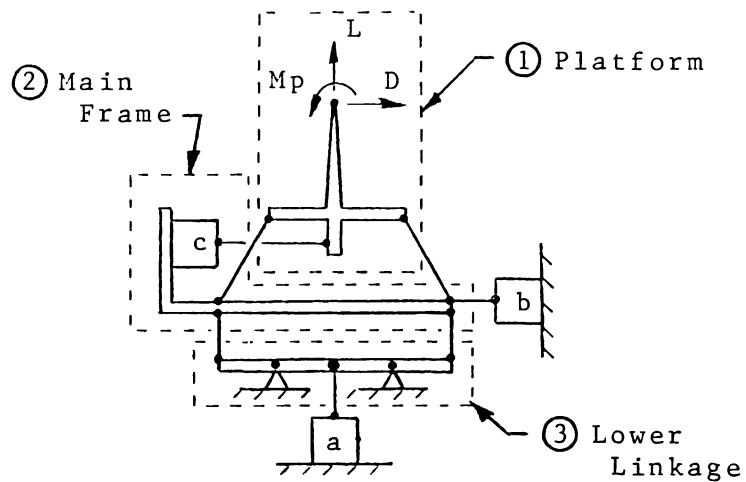


Fig. 16. Pyramidal balance components.

Three Component Balance:

To develop the static equations for the three component system, begin at the platform and continue downward through the balance. The free body diagram of the platform is shown in Figure 17:

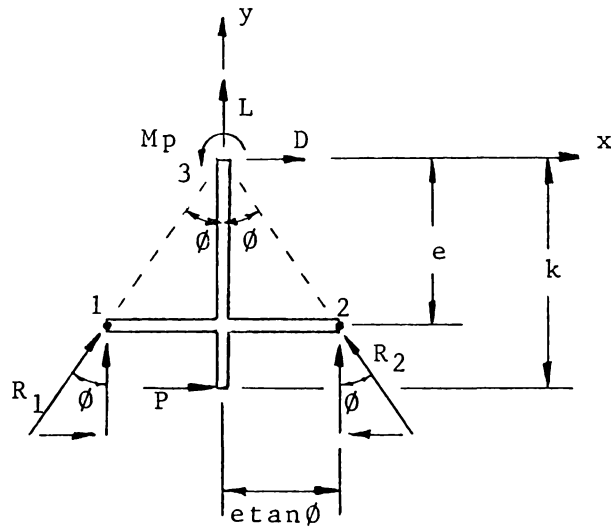


Fig. 17. Platform free body diagram: three component.

Where, $L = \text{Lift}$

$D = \text{Drag}$

$M_p = \text{Pitching moment}$

Summing the forces in the y-direction:

$$L + (R_1 + R_2)\cos\phi = 0.0 \quad 3.1$$

Summing the forces in the x-direction:

$$D + (R_1 - R_2)\sin\phi + P = 0.0 \quad 3.2$$

Summing the moments at point 1:

$$M_p + P(k - e) + R_2(2e\tan\phi)\cos\phi + Letan\phi - De = 0.0$$

rearranging and reducing the previous equation gives:

$$M_p + Pk - Pe + 2R_2e\sin\phi + Letan\phi - De = 0.0 \quad 3.3$$

Substitute equations 3.1 and 3.2 into 3.3 to eliminate D and L:

$$P = - M_p/k \quad 3.4$$

Equation 3.4 gives proof that the reaction P is uncoupled and is a function of only the pitching moment. With equation 3.4, equations 3.1 and 3.2 can be solved for R_1 and R_2 :

$$R_1 = - L/(2\cos\theta) - D/(2\sin\theta) + M_p/(2k\sin\theta) \quad 3.5$$

$$R_2 = - L/(2\cos\theta) + D/(2\sin\theta) - M_p/(2k\sin\theta) \quad 3.6$$

The relations R_1 and R_2 above represent the axial loads in the pyramidal links.

Moving down the system, to determine the reactions on the second sub-system, the main frame free body diagram is shown in Figure 18.

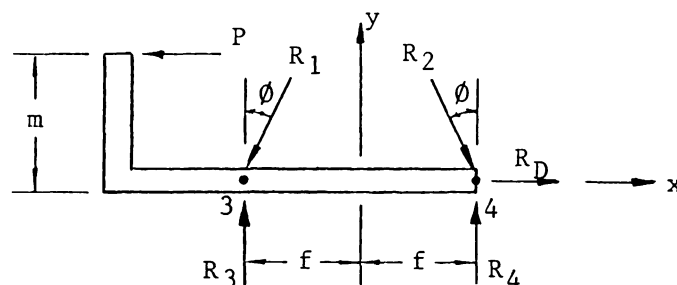


Fig. 18. Main frame free body diagram: three component.

Summing the forces in the x-direction gives:

$$R_D - P + (R_2 - R_1)\sin\theta = 0.0$$

Substitution of equations 3.4, 3.5, and 3.6 reduces the above equation to:

$$R_D = - D \quad 3.7$$

Thus, the drag load cell will read only the drag force.

Summing the forces in the y-direction gives:

$$R_3 + R_4 - (R_1 + R_2)\cos\theta = 0.0 \quad 3.8$$

Summing the moments about point 3 gives:

$$- P_m + R_2\cos\theta(2f) - R_4(2f) = 0.0 \quad 3.9$$

Using equations 3.4, 3.5, and 3.6, solve equations 3.8 and 3.9 for R_3 and R_4 :

$$R_3 = - L/2 - D/(2\tan\theta) + M_p/(2k\tan\theta) - M_{pm}/(2kf) \quad 3.10$$

$$R_4 = - L/2 + D/(2\tan\theta) - M_p/(2k\tan\theta) + M_{pm}/(2kf) \quad 3.11$$

Applying R_3 and R_4 to the lower lever system:

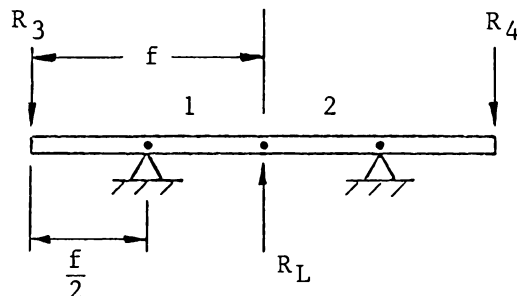


Fig. 19. Lower lever system: three component.

Thus, the lift reaction, R_L , is:

$$R_L = L \quad 3.12$$

Therefore, load cells (a), (b), and (c) shown in Figure 16 are uncoupled and will read only the lift, drag, and pitch loads, respectively.

Six Component Balance:

Now a static analysis will be performed on the general six component pyramidal balance.

First, the direction components, dimensions, and angles are established for any given pyramidal link in Figure 20:

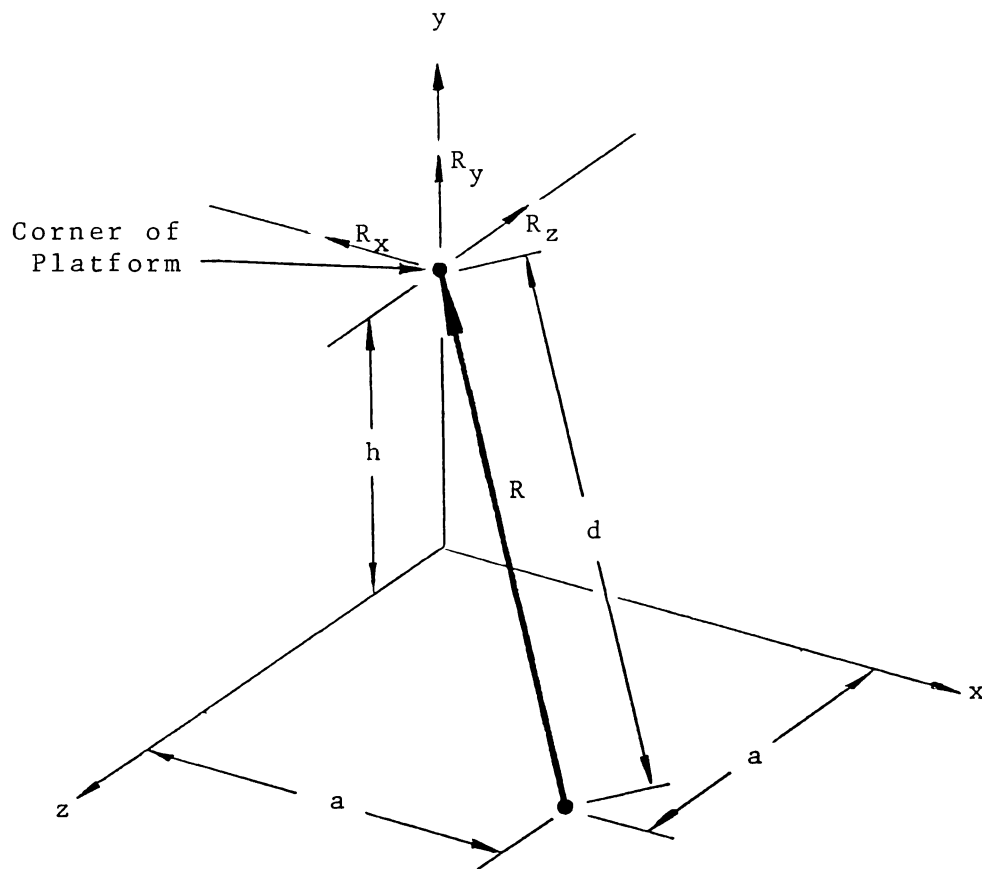


Fig. 20. Pyramidal link dimensions: six component.

Therefore,

$$\begin{aligned} R_x &= Ra/d \\ R_y &= Rh/d \\ R_z &= Ra/d \end{aligned}$$

Thus,

$$Ra/d = R_x = R_z = R_y a/h \quad 3.13$$

where,

$$\begin{aligned} d &= \text{link length} \\ h &= \text{link height} \\ a &= \text{link dimension in the x-z plane} \end{aligned}$$

The free body diagram of the six component balance platform is shown below in Figure 21. Each link is assumed to be in compression and the applied forces and moments are in the positive x-, y-, and z-directions.

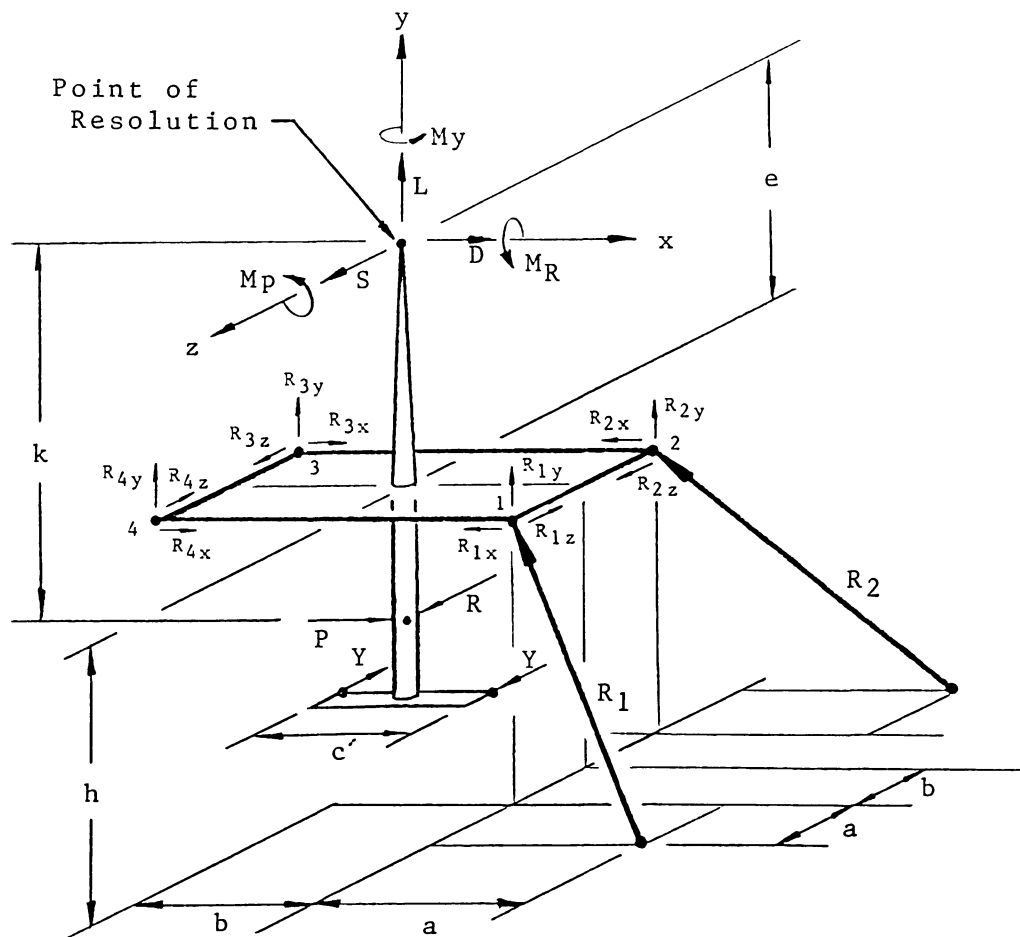


Fig. 21. Platform free body diagram: six component.

Where, R_1, R_2, R_3, R_4 = link reactions
 P = pitch moment reaction
 R = roll moment reaction
 Y = yaw moment reaction

For equilibrium:

Summing the forces in the x-direction gives:

$$D - R_{1x} - R_{2x} + R_{3x} + R_{4x} + P = 0.0 \quad 3.14$$

Summing the forces in the y-direction gives:

$$L + R_{1y} + R_{2y} + R_{3y} + R_{4y} = 0.0 \quad 3.15$$

Summing the forces in the z-direction gives:

$$S - R_{1z} + R_{2z} + R_{3z} - R_{4z} + R = 0.0 \quad 3.16$$

Summing the moments in the x-direction about the line 2-3:

$$M_R - Lb + Se - Rk + Re - 2R_{4y}b - 2R_{1y}b = 0.0 \quad 3.17$$

Summing the moments in the y-direction about point 1:

$$M_y - Db + Sb + 2R_{2x}b - 2R_{3x}b + 2R_{3z}b - 2R_{4z}b \\ - Yc' - Pb + Rb = 0.0 \quad 3.18$$

Summing the moments in the z-direction about the line 1-2:

$$M_p - Lb - De + Pk - Pe - 2R_{3y}b - 2R_{4y}b = 0.0 \quad 3.19$$

It would now be helpful to recast the above equations, 3.14 through 3.19, in terms of R_1 , R_2 , R_3 , and R_4 to reduce the number of equations to work with. From equation 3.13, the following relations are found:

$$R_1 = R_{1x}d/a = R_{1y}d/h = R_{1z}d/a \quad 3.20$$

$$R_2 = R_{2x}d/a = R_{2y}d/h = R_{2z}d/a \quad 3.21$$

$$R_3 = R_{3x}d/a = R_{3y}d/h = R_{3z}d/a \quad 3.22$$

$$R_4 = R_{4x}d/a = R_{4y}d/h = R_{4z}d/a \quad 3.23$$

Substituting equations 3.20 through 3.23 into equations 3.14 through 3.19 yields:

$$(D + P)d/a - R_1 - R_2 + R_3 + R_4 = 0.0 \quad 3.24$$

$$Ld/h + R_1 + R_2 + R_3 + R_4 = 0.0 \quad 3.25$$

$$(R + S)d/a - R_1 + R_2 + R_3 - R_4 = 0.0 \quad 3.26$$

$$M_R - Lb + Se - Rk + Re - (R_1 + R_4)(2bh)/d = 0.0 \quad 3.27$$

$$M_y - Db + Sb - Yc' - Pb + Rb + (2ab)(R_2 - R_4)/d = 0.0 \quad 3.28$$

$$M_p - Lb - De + Pk - Pe - (2bh)(R_3 + R_4)/d = 0.0 \quad 3.29$$

In anticipation of the next few steps, a geometric relation is established. Viewing a projection in the x-y plane of the platform free body diagram:

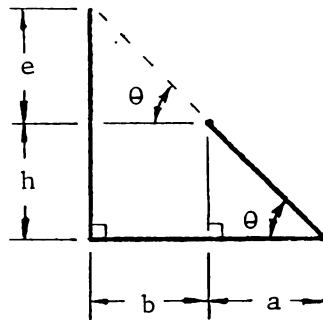


Fig. 22. Balance dimension relationships.

Thus, by similar triangles,

$$(e + h)/(b + a) = h/a = \tan\theta$$

This reduces to: $ae = bh$ 3.30

Substituting equations 3.24, 3.25, 3.26, and 3.30 into equations 3.27, 3.28, and 3.29, yields:

$$R = M_R/k \quad 3.31$$

$$Y = M_y/c' \quad 3.32$$

$$P = - M_p/k \quad 3.33$$

Thus, the moment load cells are uncoupled and separated from the rest of the loads.

Placing equations 3.31, 3.32, and 3.33 back into 3.24, 3.25, and 3.26 gives:

$$Dd/a - M_p d/(ka) - R_1 - R_2 + R_3 + R_4 = 0.0 \quad 3.34$$

$$Ld/h + R_1 + R_2 + R_3 + R_4 = 0.0 \quad 3.35$$

$$Sd/a + M_R d/(ka) - R_1 + R_2 + R_3 - R_4 = 0.0 \quad 3.36$$

With four unknowns and three equations, an alternate method of solution must be found. Here, it is assumed that the balance's geometry is symmetric. Consequently, there are symmetries in the way the loads are distributed. Consider projections of the platform onto each of the following three planes: x-y, y-z, and x-z. For the x-y plane:

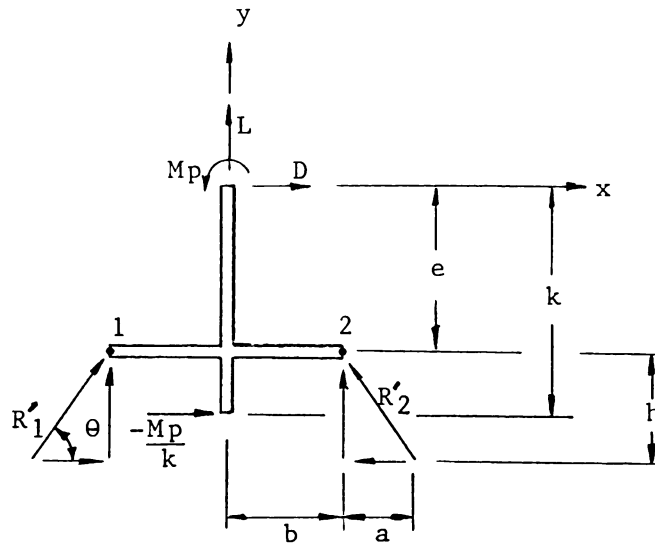


Fig. 23. Platform free body diagram: x-y plane.

Summing the moments about point 2 gives:

$$R_1' \sin \theta = -L/2 - Dh/(2a) + M_p h/(2ak) \quad 3.37$$

Summing the moments about point 1 gives:

$$R_2' \sin \theta = -L/2 + Dh/(2a) - M_p h/(2ak) \quad 3.38$$

Summing the forces in the x-direction gives:

$$R_1' \cos \theta = D/2 - M_p/(2k)$$

$$R_2' \cos \theta = -D/2 + M_p/(2k)$$

For the y-z plane:

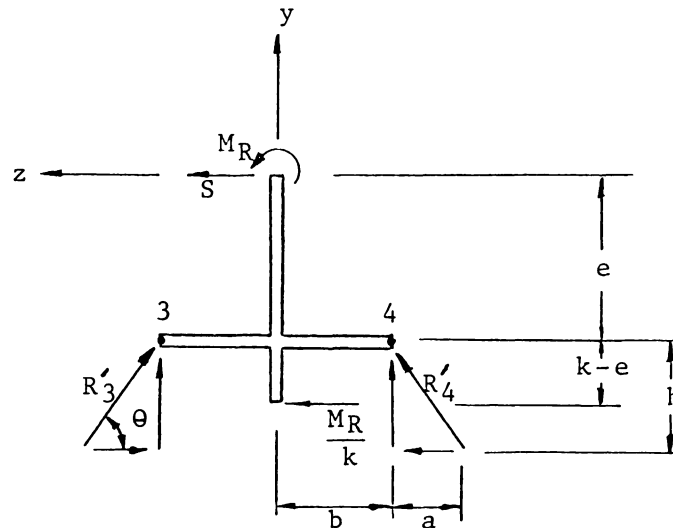


Fig. 24. Platform free body diagram: y-z plane.

Summing the moments about point 4 gives:

$$R_3' \sin \theta = Sh/(2a) + M_R h/(2ak) \quad 3.39$$

Summing the moments about point 3 gives:

$$R_4' \sin \theta = -Sh/(2a) - M_R h/(2ak) \quad 3.40$$

Summing the forces in the z-direction gives:

$$R_3' \cos \theta = S/2 + M_R/(2k)$$

$$R_4' \cos \theta = -S/2 - M_R/(2k)$$

For the x-z plane: (looking downward on the balance)

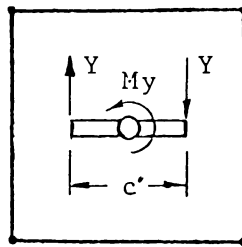


Fig. 25. Platform free body diagram: x-z plane.

where, as previously found, $Y = M_y/c'$.

It is clear that M_y in Figure 25 is reacted entirely by Y and will have no effect on the link reactions. Because of symmetry, each component of R' can be equally distributed along the edge that it acts upon. This is shown in Figure 26:

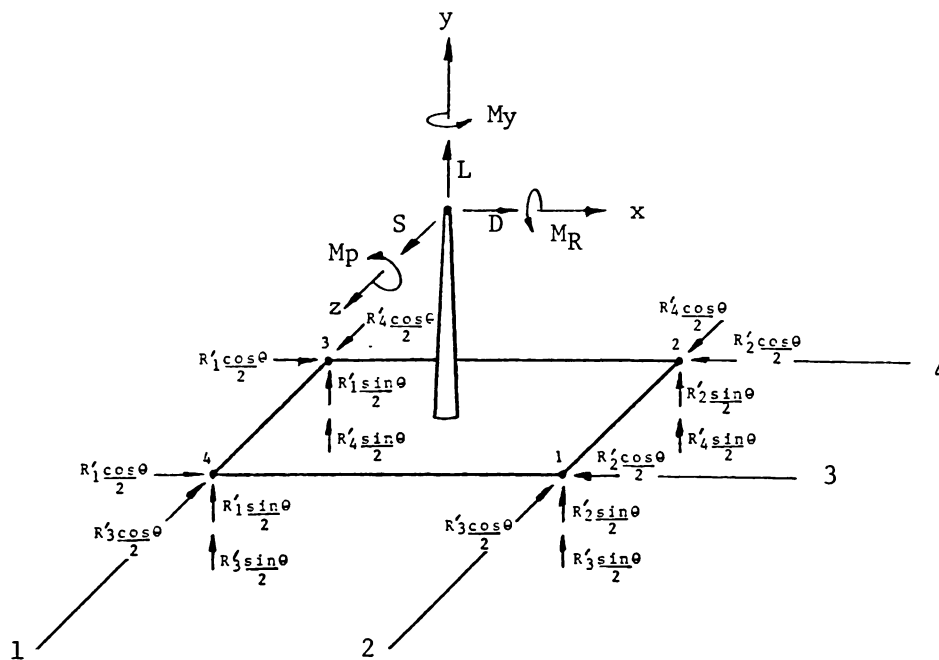


Fig. 26. Symmetric force components on platform.

By comparison with the first free body diagram of the platform (Figure 21), the vertical components of the link reactions are:

$$R_{1y} = (R_2'\sin\theta + R_3'\sin\theta) / 2 \quad 3.41$$

$$R_{2y} = (R_2'\sin\theta + R_4'\sin\theta) / 2 \quad 3.42$$

$$R_{3y} = (R_1'\sin\theta + R_4'\sin\theta) / 2 \quad 3.43$$

$$R_{4y} = (R_1'\sin\theta + R_3'\sin\theta) / 2 \quad 3.44$$

Once these vertical components are found, then the axial link loads can be found by equation 3.13. Note that the link forces cannot be correctly found from the summation of the horizontal components that lie in the x-z plane. The true horizontal components (R_x and R_z) can only be found from the vertical component, R_y . This is because the previous diagram created by the use of symmetry (Figure 26) does not account for any forces in the horizontal x-z plane that may cancel each other. On the other hand, the summation of the vertical forces by symmetry will give the true vertical component (R_z) because the lines of action of R_{1z} , R_{2z} , R_{3z} , and R_{4z} do not intersect. Therefore, no components of force are omitted or canceled.

Substituting equations 3.37, 3.38, 3.39, and 3.40 into equations 3.41, 3.42, 3.43, and 3.44 and using equation 3.13 yields:

$$R_{1y} = [- La/h + D + S - M_p/k + M_R/k] h / (4a) \quad 3.45$$

$$R_{1x} = R_{1z} = [- La/h + D + S - M_p/k + M_R/k] / 4 \quad 3.46$$

$$R_{2y} = [- La/h + D - S - M_p/k - M_R/k] h / (4a) \quad 3.47$$

$$R_{2x} = R_{2z} = [- La/h + D - S - M_p/k - M_R/k] / 4 \quad 3.48$$

$$R_{3y} = [- La/h - D - S + M_p/k - M_R/k] h/(4a) \quad 3.49$$

$$R_{3x} = R_{3z} = [- La/h - D - S + M_p/k - M_R/k] /4 \quad 3.50$$

$$R_{4y} = [- La/h - D + S + M_p/k + M_R/k] h/(4a) \quad 3.51$$

$$R_{4x} = R_{4z} = [- La/h - D + S + M_p/k + M_R/k] /4 \quad 3.52$$

Finally, by again using equation 3.13, the axial forces in the links are found to be:

$$R_1 = [- La/h + D + S - M_p/k + M_R/k] d/(4a) \quad 3.53$$

$$R_2 = [- La/h + D - S - M_p/k - M_R/k] d/(4a) \quad 3.54$$

$$R_3 = [- La/h - D - S + M_p/k - M_R/k] d/(4a) \quad 3.55$$

$$R_4 = [- La/h - D + S + M_p/k + M_R/k] d/(4a) \quad 3.56$$

Note that these relations for the axial forces in the links satisfy equilibrium equations 3.34, 3.35, and 3.36.

Equations 3.53 through 3.56 can be succinctly written in matrix notation as:

$$\{R\} = [A]\{B\}d/(4a) \quad 3.57$$

where,

$$\{R\} = \begin{Bmatrix} R_1 \\ R_2 \\ R_3 \\ R_4 \end{Bmatrix}, \quad \{B\} = \begin{Bmatrix} L \\ D \\ S \\ M_p/k \\ M_R/k \end{Bmatrix}$$

and

$$[A] = \begin{bmatrix} -1 & 1 & 1 & -1 & 1 \\ -1 & 1 & -1 & -1 & -1 \\ -1 & -1 & -1 & 1 & -1 \\ -1 & -1 & 1 & 1 & 1 \end{bmatrix}$$

Moving down the system, the free body diagram of the main frame appears as in Figure 27:

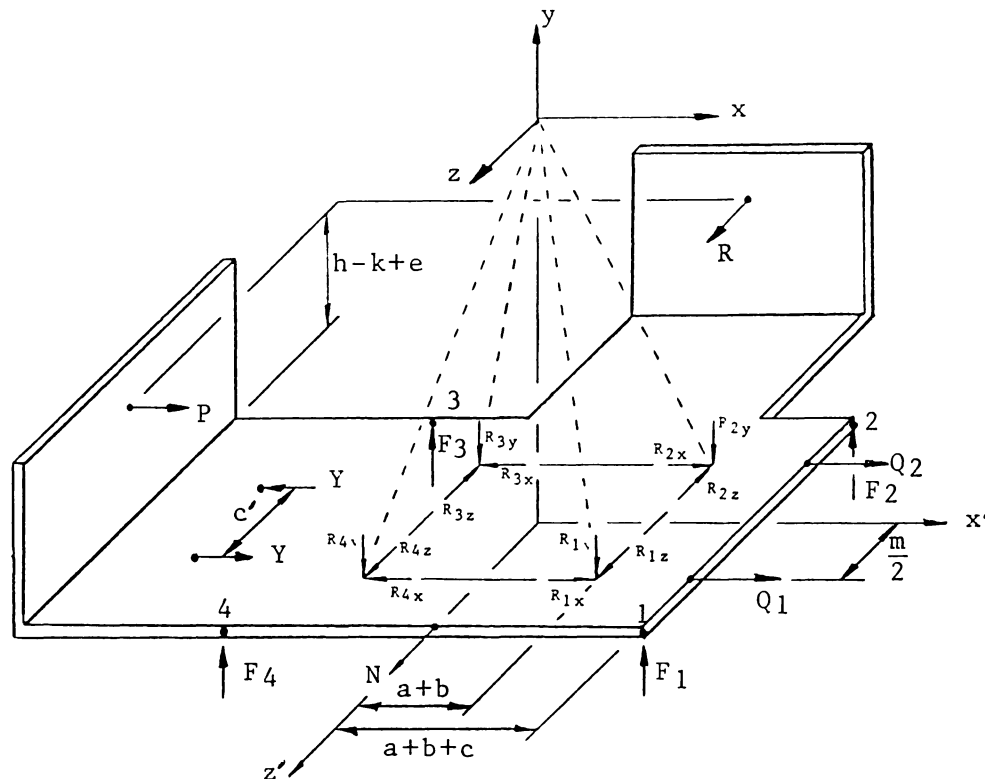


Fig. 27. Main frame free body diagram: six component.

Summing the forces in the x-direction:

$$P + R_{1x} + R_{2x} - R_{3x} - R_{4x} + Q_1 + Q_2 = 0.0 \quad 3.58$$

Summing the forces in the y-direction:

$$F_1 + F_2 + F_3 + F_4 - R_{1y} - R_{2y} - R_{3y} - R_{4y} = 0.0 \quad 3.59$$

Summing the forces in the z-direction:

$$R_{1z} - R_{2z} - R_{3z} + R_{4z} - R + N = 0.0 \quad 3.60$$

Summing the moments about the x'-axis:

$$\begin{aligned} (R_{1y} + R_{4y})(a + b) - (R_{2y} + R_{3y})(a + b) \\ - (F_1 + F_4)(a + b + c) + (F_2 + F_3)(a + b + c) \\ - R(h - k + e) = 0.0 \quad 3.61 \end{aligned}$$

Summing the moments about the y-axis:

$$Yc' + Q_1m/2 - Q_2m/2 + (R_{1x} + R_{3x} + R_{2z} + R_{4z})(a + b) - (R_{1z} + R_{3z} + R_{2x} + R_{4x})(a + b) = 0.0 \quad 3.62$$

Summing the moments about the z'-axis:

$$- P(h - k + e) + (F_1 + F_2)(a + b + c) - (F_3 + F_4)(a + b + c) + (R_{3y} + R_{4y})(a + b) - (R_{1y} + R_{2y})(a + b) = 0.0 \quad 3.63$$

Substitute equations 3.31, 3.32, 3.33, and 3.45 through 3.52 into equations 3.58, 3.59, 3.60, 3.61, 3.62, and 3.63 to get:

$$D + Q_1 + Q_2 = 0.0 \quad 3.64$$

$$F_1 + F_2 + F_3 + F_4 + L = 0.0 \quad 3.65$$

$$S = -N \quad 3.66$$

$$S(h + e) + (a+b+c)(-F_1 + F_2 + F_3 - F_4) + M_R = 0.0 \quad 3.67$$

$$M_y + Q_1m/2 - Q_2m/2 = 0.0 \quad 3.68$$

$$M_p + (a+b+c)(F_1 + F_2 - F_3 - F_4) - D(h + e) = 0.0 \quad 3.69$$

Solving 3.68 and 3.64 for Q_1 and Q_2 yields:

$$Q_1 = -M_y/m - D/2 \quad 3.70$$

$$Q_2 = M_y/m - D/2 \quad 3.71$$

This leaves three equations (3.65, 3.67, and 3.69) and four unknowns (F_1 , F_2 , F_3 , and F_4). Consequently, symmetry will be used to provide an additional equation, as was done with the platform analysis.

For the x-y plane:

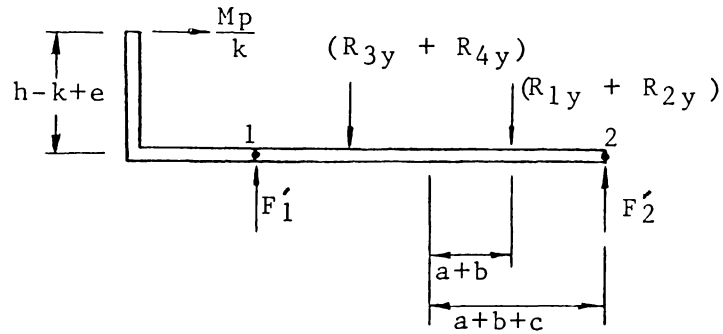


Fig. 28. Main frame free body diagram: x-y plane.

Summing the moments at point 2 and simplify:

$$F_1' = -L/2 - D(h + e)/[2(a+b+c)] + M_p/[2(a+b+c)] \quad 3.72$$

Summing the forces in the y-direction:

$$F_2' = -L/2 + D(h + e)/[2(a+b+c)] - M_p/[2(a+b+c)] \quad 3.73$$

Likewise, for the y-z plane:

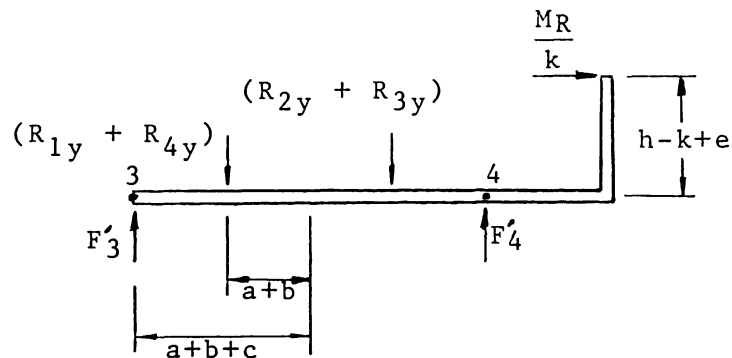


Fig. 29. Main frame free body diagram: y-z plane.

Summing the moments about point 4 and simplify:

$$F_3' = -L/2 + S(h + e)/[2(a+b+c)] + M_R/[2(a+b+c)] \quad 3.74$$

Summing the forces in the y-direction:

$$F_4' = -L/2 - S(h + e)/[2(a+b+c)] - M_R/[2(a+b+c)] \quad 3.75$$

Now, due to geometric symmetry and the orthogonality of the applied forces and moments, F_1' , F_2' , F_3' , and F_4' are distributed equally along lines (1), (2), (3), and (4) as shown in Figure 30.

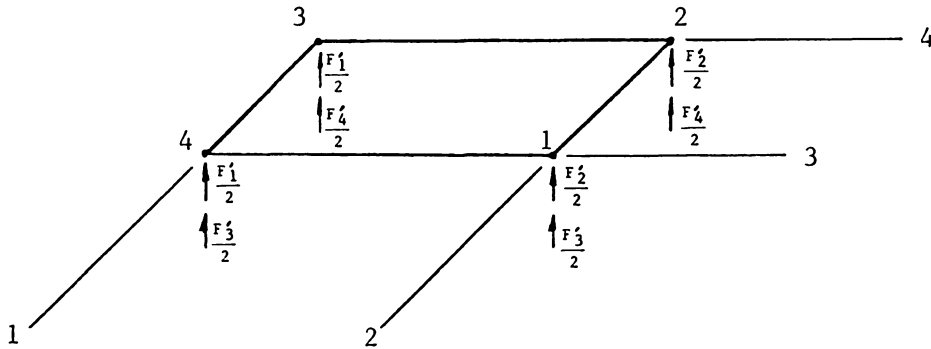


Fig. 30. Symmetric force components on main frame.

Setting the vertical forces in Figure 27 equal to those of Figure 30,

$$F_1 = (F_2' + F_3')/2 \quad 3.76$$

$$F_2 = (F_2' + F_4')/2 \quad 3.77$$

$$F_3 = (F_1' + F_4')/2 \quad 3.78$$

$$F_4 = (F_1' + F_3')/2 \quad 3.79$$

Note that the lift component will be omitted from F_3' and F_4' since it was already accounted for in F_1' and F_2' .

Finally, substituting equations 3.72 through 3.75 into 3.76 through 3.79 yields:

$$F_1 = [-L(a+b+c) + (D+S)(h+e) - M_p + M_R] / [4(a+b+c)] \quad 3.80$$

$$F_2 = [-L(a+b+c) + (D-S)(h+e) - M_p - M_R] / [4(a+b+c)] \quad 3.81$$

$$F_3 = [-L(a+b+c) - (D+S)(h+e) + M_p - M_R] / [4(a+b+c)] \quad 3.82$$

$$F_4 = [-L(a+b+c) - (D-S)(h+e) + M_p + M_R] / [4(a+b+c)] \quad 3.83$$

As a final check, equations 3.80 through 3.83 can be substituted back into the equilibrium equations 3.65, 3.67,

and 3.69. It will be seen that the equations are satisfied.

Finally, a second equilibrium analysis can be conducted that involves the overall system; treating both the platform and the main frame as a single system. In solving for F_1 through F_4 with this approach it can be shown that the relations found will confirm equations 3.80 through 3.83. Using these equations, the forces in the lever system can be defined.

As was shown in the pyramidal concepts (Section A) the lever system on the six component balance is configured as in Figure 31.

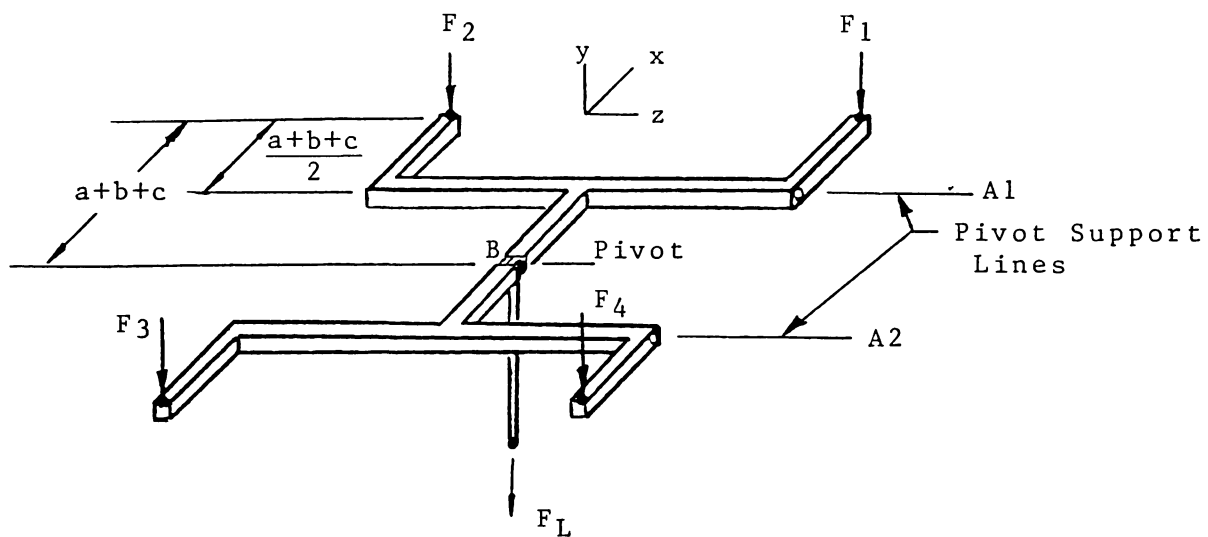


Fig. 31. Lower lever system: six component.

Viewing the x-y plane of half the symmetric linkage, the free body diagram is shown in Figure 32:

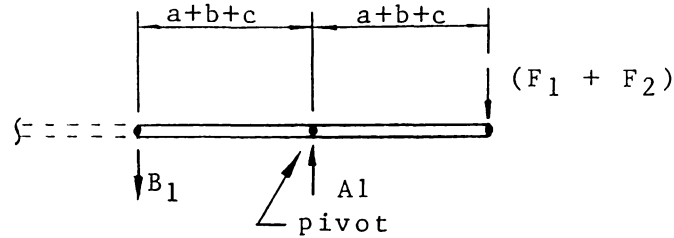


Fig. 32. Lower lever system: symmetric half in x-y plane.

Summing the moments about line A1 and simplifying gives:

$$B_1 = - L/2 + D(h + e)/[2(a+b+c)] - M_p/[2(a+b+c)] \quad 3.84$$

Likewise, on the other half of the lever system:

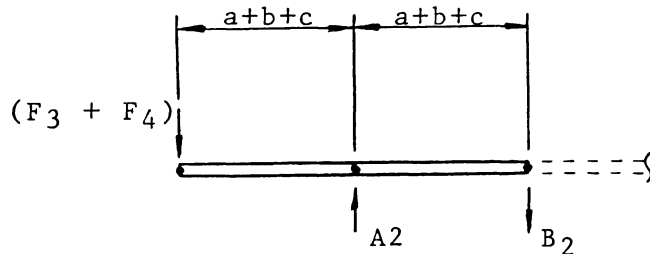


Fig. 33. Lower lever system: symmetric half in x-y plane.

Summing the moments about line A2 and simplify:

$$B_2 = - L/2 - D(h + e)/[2(a+b+c)] + M_p/[2(a+b+c)] \quad 3.85$$

$$\text{But, } F_L = B_1 + B_2 \quad 3.86$$

Thus, with equations 3.84 and 3.85,

$$F_L = - L \quad 3.87$$

This shows that the lift load cell is uncoupled and will indicate only the force due to lift, as was discussed in the Section A of this chapter.

Similarly, the drag/yaw frame appears as:

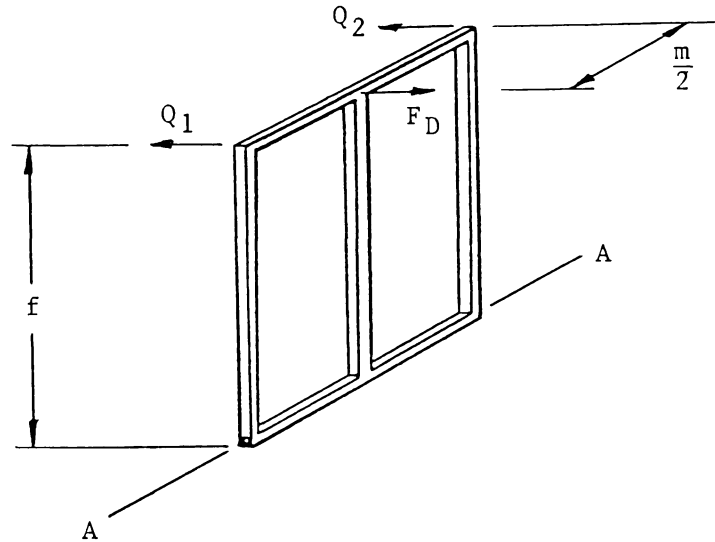


Fig. 34. Drag/Yaw frame: six component.

Summing the moments along line AA and using equations 3.70 and 3.71:

$$F_D = - D \quad 3.88$$

Therefore, as seen in equations 3.31, 3.32, 3.33, 3.66, 3.87, and 3.88, all the forces and moments are proven to be separated and uncoupled for the pyramidal force balance concept.

C. Uncertainty Analysis:

The total uncertainty of wind tunnel data is comprised of several elements. The following diagram illustrates these elements.

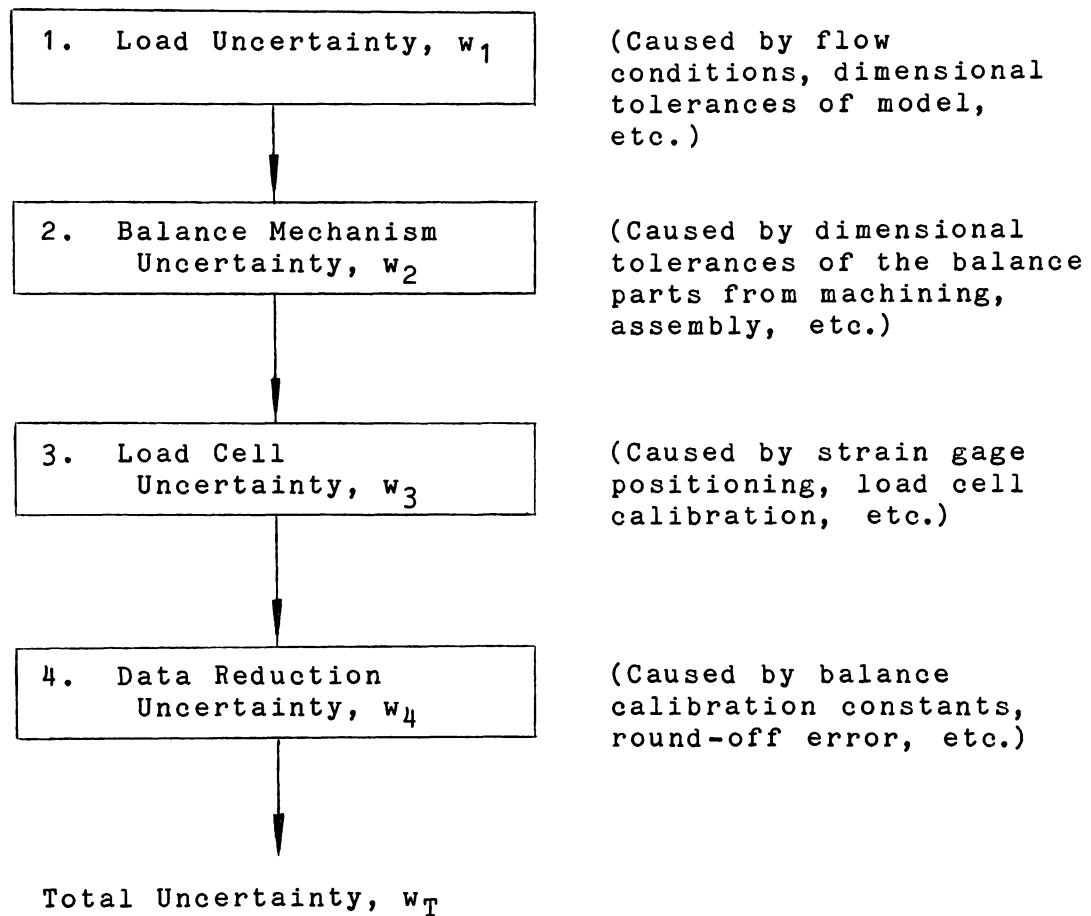


Fig. 35. Uncertainty diagram.

The total uncertainty (w_T) is defined as:

$$w_T = [w_1^2 + w_2^2 + w_3^2 + w_4^2]^{1/2}$$

All the uncertainty analyses to be presented will concentrate on the balance mechanism, w_2 . It should be remembered that w_2 is only a portion of the total uncertainty associated with the final wind tunnel data.

Minimizing this uncertainty during the construction and assembly of the balance allows the tunnel engineer to neglect the effect of w_2 on the final data.

The uncertainty of the measured reactions is defined using the method presented by J. P. Holman [10]. In general, this method provides that, if the result J of a measurement is a given function of the independent variables $x_1, x_2, x_3, \dots, x_n$, or:

$$J = J(x_1, x_2, x_3, \dots, x_n),$$

Then the uncertainty in J (the result), w_J , is a function of the known uncertainties in the n independent variables $w_1, w_2, w_3, \dots, w_n$. The uncertainty relationship for the result (J), w_J , can thus be written as:

$$w_J = [(\partial J / \partial x_1)^2 (w_1)^2 + (\partial J / \partial x_2)^2 (w_2)^2 + \dots + (\partial J / \partial x_n)^2 (w_n)^2]^{1/2} \quad 3.89$$

From the pyramidal balance static analysis, the general axial loads in the pyramidal links, and the lower links, are given by equations 3.57 and 3.80 through 3.83.

It is readily seen that these forces will be influenced by any tolerance allowances on the dimensions:

$a, b, c, d, e, h,$ and k

The uncertainty tolerances, w_i , with $i = a, b, c, d, e, h, k$ for each dimension are defined to be:

a: w_a
 b: w_b
 c: w_c
 d: w_d
 e: w_e
 h: w_h
 k: w_k

These tolerances are presumed to be known or determinable (i.e. they are specified according to the accuracy of the machining work which was done on the balance). As discussed at the beginning of this section, the output uncertainties considered here are useful in that they can help define the accuracy to which the parts of the balance must be machined and/or assembled.

To assist with the derivation of the balance uncertainties, the following quantities are defined:

L, D, S = Lift, Drag, and Side forces

M_p, M_R, M_y = Pitch, Roll, and Yaw moments

$$A = D + S - M_p/k + M_R/k \quad 3.90$$

$$B = M_p - M_R \quad 3.91$$

$$E = D - S - M_p/k - M_R/k \quad 3.92$$

$$F = M_p + M_R \quad 3.93$$

$$G = (w_a/a)^2 + (w_d/d)^2 \quad 3.94$$

$$H = (w_h/h)^2 + (w_d/d)^2 \quad 3.95$$

$$I = (w_b/b)^2 + (w_{c'}/c')^2 \quad 3.96$$

$$T = M_p^2 + M_R^2 \quad 3.97$$

$$U = D - M_p/k \quad 3.98$$

$$V = S + M_R/k \quad 3.99$$

The uncertainties of the pyramidal link reactions (R) will be discussed first. It is assumed that the applied load (forces and moments) uncertainties are independent of the balance. Therefore, the partial derivatives of $L, D, S, M_p, M_R,$ and M_y are zero. The partial derivatives of R_1 with respect to the dimensions $a, d, h,$ and k are found from equations 3.57 as:

$$\partial R_1 / \partial a = - (dA) / (4a^2)$$

$$\partial R_1 / \partial d = - L / (4h) + A / (4a)$$

$$\partial R_1 / \partial h = Ld / (4h^2)$$

$$\partial R_1 / \partial k = dB / (4ak^2)$$

$$\partial R_1 / \partial b = \partial R_1 / \partial c = \partial R_1 / \partial e = 0.0$$

Substituting these values into equation 3.89 to find the uncertainty of R_1 , gives:

$$w_{R1} = \{ [-(dA)/(4a^2)]^2 [w_a]^2 + [-L/(4h) + A/(4a)]^2 [w_d]^2 + [Ld/(4h^2)]^2 [w_h]^2 + [dB/(4ak^2)]^2 [w_k]^2 \}^{1/2}$$

After some algebraic manipulations and making use of equations 3.90 through 3.99, a final form for w_{R1} is found to be:

$$w_{R1} = d [(Ah)^2 G - 2LAah(w_d/d)^2 + (La)^2 H + (Bhw_k)^2 / k^4]^{1/2} (4ah)^{-1} \quad 3.100$$

Similarly, the uncertainties of R_2 , R_3 , and R_4 can be found:

$$w_{R2} = d [(Eh)^2 G - 2LEah(w_d/d)^2 + (La)^2 H + (Fhw_k)^2 / k^4]^{1/2} (4ah)^{-1} \quad 3.101$$

$$w_{R3} = d [(Ah)^2 G + 2LAah(w_d/d)^2 + (La)^2 H + (Bhw_k)^2 / k^4]^{1/2} (4ah)^{-1} \quad 3.102$$

$$w_{R4} = d [(Eh)^2 G + 2LEah(w_d/d)^2 + (La)^2 H + (Fhw_k)^2 / k^4]^{1/2} (4ah)^{-1} \quad 3.103$$

Now, the uncertainties of the various force and moment reactions can be found. The notation to be used for these is:

Pitch reaction: w_P
 Roll reaction : w_R
 Yaw reaction : w_Y
 Lift reaction : w_{FL}
 Drag reaction : w_{FD}
 Side reaction : w_N

Pitch Moment Reaction

For the uncertainty of the pitch reaction, use equation 3.24:

$$P = (a/d)(R_1 + R_2 - R_3 - R_4) - D$$

Find the partial derivatives of P with respect to a, d, R₁, R₂, R₃, and R₄.

$$\begin{aligned} \partial P / \partial a &= (R_1 + R_2 - R_3 - R_4) / d \\ &= U/a \end{aligned}$$

$$\begin{aligned} \partial P / \partial d &= - (R_1 + R_2 - R_3 - R_4) a / d^2 \\ &= - U/d \end{aligned}$$

$$\partial P / \partial R_1 = \partial P / \partial R_2 = - \partial P / \partial R_3 = - \partial P / \partial R_4 = a/d$$

From equation 3.89, the uncertainty of the pitch reaction is written as:

$$\begin{aligned} w_p &= [(Uw_a/a)^2 + (Uw_d/d)^2 \\ &\quad + (a/d)^2 (w_{R1}^2 + w_{R2}^2 + w_{R3}^2 + w_{R4}^2)]^{1/2} \end{aligned}$$

After some algebraic manipulations and making use of equations 3.90 through 3.99, a final form for w_p is found to be:

$$\begin{aligned} w_p &= (1/2) [G(5U^2 + V^2) + (La/h)^2 H \\ &\quad + (w_k^2/k^4) T]^{1/2} \end{aligned} \quad 3.104$$

Roll Moment Reaction

From the static analysis of the platform, the roll reaction, R, was given by equation 3.26:

$$R = (a/d)(R_1 - R_2 - R_3 + R_4) - S$$

The partial derivatives are:

$$\begin{aligned} \partial R / \partial a &= (R_1 - R_2 - R_3 + R_4) / d \\ &= V/a \end{aligned}$$

$$\begin{aligned}\partial R/\partial d &= - (a/d^2)(R_1 - R_2 - R_3 + R_4) \\ &= - V/d\end{aligned}$$

$$\partial R/\partial R_1 = \partial R/\partial R_2 = - \partial R/\partial R_3 = - \partial R/\partial R_4 = a/d$$

Similar to the pitch reaction, the final equation for the uncertainty of the roll reaction is then found to be:

$$\begin{aligned}w_R &= (1/2)[G(U^2 + 5V^2) + (La/h)^2 H \\ &\quad + (w_k^2/k^4)T]^{1/2} \quad 3.105\end{aligned}$$

Yaw Moment Reaction

The yaw uncertainty can be determined from equation 3.28:

$$Y = M_y/c' + (b/c')[- D + S - P + R + (2a/d)(R_2 - R_4)]$$

The partial derivatives are:

$$\begin{aligned}\partial Y/\partial a &= (2b)(R_2 - R_4)/(c'd) \\ &= bE/(c'a)\end{aligned}$$

$$\begin{aligned}\partial Y/\partial b &= (- D + S - M_p/k + M_R/k + E)/c' \\ &= - 2M_p/(c'k)\end{aligned}$$

$$\begin{aligned}\partial Y/\partial c' &= - b[- D + S - M_p/k + M_R/k + E]/c'^2 - M_y/c'^2 \\ &= - (2bM_p/k + M_y)/c'^2\end{aligned}$$

$$\begin{aligned}\partial Y/\partial d &= - (2ab)(R_2 - R_4)/(c'd^2) \\ &= - bE/(c'd)\end{aligned}$$

$$\partial Y/\partial P = - \partial Y/\partial R = b/c'$$

$$\partial Y/\partial R_2 = - \partial Y/\partial R_4 = 2ab/(c'd)$$

Therefore,

$$\begin{aligned}w_Y &= \{ [(bEw_a)/(c'a)]^2 + [(2M_p w_b)/(c'k)]^2 \\ &\quad + [(2bM_p/k + M_y)(w_{c'})]^2/c'^4 + [(bEw_d)/(c'd)]^2 \\ &\quad + (b/c')^2(w_p^2 + w_R^2) + (2ab)^2(w_{R2}^2 \\ &\quad + w_{R4}^2)/(c'd)^2 \}^{1/2}\end{aligned}$$

This reduces to the final form of:

$$w_Y = (b/c') [3G(U^2 + V^2 - UV) + (La/h)^2 H + 4(M_p/k)^2 I + w_k^2 (T + M_p M_R)/k^4 + w_{c'}^2 (M_Y^2 + 4bM_p M_Y/k)/c'^4]^{1/2} \quad 3.106$$

Side Force Reaction

The uncertainty of the side force reaction, w_N , can be found from the main frame static analysis. Using equation 3.60:

$$N = -R_{1z} + R_{2z} + R_{3z} - R_{4z} + R$$

Since $R_z = (a/d)R$ from equation 3.13, then:

$$N = (a/d)(-R_1 + R_2 + R_3 - R_4) + R$$

After taking the partial derivatives of N with respect to a , d , R_1 , R_2 , R_3 , R_4 , and R , w_N is found to be:

$$w_N = (2)^{1/2} w_R \quad 3.107$$

Drag Force Reaction

Similar to the side force reaction, the main frame static analysis yields equation 3.58 for the drag force:

$$Q_1 + Q_2 = -R_{1x} - R_{2x} + R_{3x} + R_{4x} - P$$

Since $R_x = (a/d)R$ and $F_D = Q_1 + Q_2$, then:

$$F_D = (a/d)(-R_1 - R_2 + R_3 + R_4) - P$$

When the partial derivatives of F_D with respect to a , d , R_1 , R_2 , R_3 , R_4 , and P , are found and substituted into the general formula for the uncertainty (equation 3.89), w_{FD} is determined to be:

$$w_{FD} = (2)^{1/2} w_p \quad 3.108$$

Lift Force Reaction

To find the uncertainty of the lift reaction, use F_1 , F_2 , F_3 , and F_4 given by equations 3.80 through 3.83. Take the partial derivatives of F_1 with respect to a , b , c , e , and h :

$$\begin{aligned} \partial F_1 / \partial a = \partial F_1 / \partial b = \partial F_1 / \partial c = \\ - [(D+S)(h+e) - M_p + M_R] / [4(a+b+c)^2] \end{aligned}$$

$$\partial F_1 / \partial e = \partial F_1 / \partial h = (D + S) / [4(a + b + c)]$$

The uncertainty of F_1 is then found to be:

$$\begin{aligned} w_{F1} = \{ [(D+S)(h+e) - M_p + M_R]^2 (w_a^2 + w_b^2 + w_c^2) / (a+b+c)^2 \\ + (D + S)^2 (w_h^2 + w_e^2) \}^{1/2} [4(a+b+c)]^{-1} \end{aligned} \quad 3.109$$

Likewise,

$$\begin{aligned} w_{F2} = \{ [(D-S)(h+e) - M_p - M_R]^2 (w_a^2 + w_b^2 + w_c^2) / (a+b+c)^2 \\ + (D - S)^2 (w_h^2 + w_e^2) \}^{1/2} [4(a+b+c)]^{-1} \end{aligned} \quad 3.110$$

$$w_{F3} = w_{F1} \quad 3.111$$

$$w_{F4} = w_{F2} \quad 3.112$$

From the static analysis of the lower linkage, it was found that:

$$B_1 = F_1 + F_2 \quad \text{and} \quad B_2 = F_3 + F_4$$

and,

$$F_L = B_1 + B_2 = F_1 + F_2 + F_3 + F_4$$

The partial derivatives of F_L with respect to F_1 , F_2 , F_3 , and F_4 are simply:

$$\partial F_L / \partial F_1 = \partial F_L / \partial F_2 = \partial F_L / \partial F_3 = \partial F_L / \partial F_4 = 1.0$$

The uncertainty of the lift load is thus:

$$w_{FL} = (w_{F1}^2 + w_{F2}^2 + w_{F3}^2 + w_{F4}^2)^{1/2}$$

or, using equations 3.111 and 3.112,

$$w_{FL} = (2w_{F1}^2 + 2w_{F2}^2)^{1/2}$$

Finally, the lift uncertainty is found to be:

$$\begin{aligned} w_{FL} = & \{(w_a^2 + w_b^2 + w_c^2)[((D+S)(h+e) - M_p + M_R)^2 \\ & + ((D-S)(h+e) - M_p - M_R)^2][2(a+b+c)^2]^{-1} \\ & + (w_h^2 + w_e^2)(D^2 + S^2)\}^{1/2}(2a + 2b + 2c)^{-1} \end{aligned} \quad 3.113$$

Using the quantities defined in equations 3.90 through 3.99, a summary of the reaction uncertainties is listed below:

Pitch:

$$\begin{aligned} w_p = & (1/2)[G(5U^2 + V^2) + (La/h)^2H \\ & + (w_k^2/k^4)T]^{1/2} \end{aligned} \quad 3.104$$

Roll:

$$\begin{aligned} w_R = & (1/2)[G(U^2 + 5V^2) + (La/h)^2H \\ & + (w_k^2/k^4)T]^{1/2} \end{aligned} \quad 3.105$$

Yaw:

$$\begin{aligned} w_Y = & (b/c')[3G(U^2 + V^2 - UV) + (La/h)^2H + 4(M_p/k)^2I \\ & + w_k^2(T + M_p M_R)/k^4 + w_{c'}^2(M_y^2 \\ & + 4bM_p M_y/k)/c'^4]^{1/2} \end{aligned} \quad 3.106$$

Side:

$$w_N = (2)^{1/2}w_R \quad 3.107$$

Drag:

$$w_{FD} = (2)^{1/2}w_p \quad 3.108$$

Lift:

$$\begin{aligned} w_{FL} = & \{(w_a^2 + w_b^2 + w_c^2)[((D+S)(h+e) - M_p + M_R)^2 \\ & + ((D-S)(h+e) - M_p - M_R)^2][2(a+b+c)^2]^{-1} \\ & + (w_h^2 + w_e^2)(D^2 + S^2)\}^{1/2}(2a + 2b + 2c)^{-1} \end{aligned} \quad 3.113$$

Appendix A includes a numerical example which demonstrates the use of these equations.

Uncertainty Assessment - Pyramidal Balance

To draw any conclusions about equations 3.104, 3.105, 3.106, 3.107, 3.108, and 3.113, a series of load and tolerance cases are considered by the variation of parameters method. A computer is used to allow repeated evaluation of the equations for each case. The numerical values for the nominal machined dimensions from the example in Appendix A are used and held constant for all of the cases. The following seven cases are considered:

1. All loads = 1.0 lb or in-lb
2. L = 10 lb All other loads = 1.0 lb or in-lb
3. D = 10 lb All other loads = 1.0 lb or in-lb
4. S = 10 lb All other loads = 1.0 lb or in-lb
5. $M_p = 10$ in-lb All other loads = 1.0 lb or in-lb
6. $M_R = 10$ in-lb All other loads = 1.0 lb or in-lb
7. $M_Y = 10$ in-lb All other loads = 1.0 lb or in-lb

Under each load case, the machined tolerances were individually varied from 0.001" to 0.1" in seven subcases, a through g:

- | | | | | |
|----|---------------------------|---------------------------------|---|------------|
| a: | All tolerances = 0.001 in | | | |
| b: | $w_b = 0.1$ in | All other tolerances = 0.001 in | | |
| c: | $w_c = 0.1$ in | " | " | = 0.001 in |
| d: | $w_{c'} = 0.1$ in | " | " | = 0.001 in |
| e: | $w_d = 0.1$ in | " | " | = 0.001 in |
| f: | $w_e = 0.1$ in | " | " | = 0.001 in |
| g: | $w_k = 0.1$ in | " | " | = 0.001 in |

These cases and subcases will yield just under three hundred different output uncertainties; or forty nine for each measured reaction. The ones that are of the most interest are the maxima and their associated tolerance subcases. This information can be plotted on a histogram as the maximum % from nominal versus case (Figure 36). Each point plotted on the histogram represents the maximum uncertainty

variance from nominal for a given load case. In the legend, the subcase tolerance that caused the maximum variance is indicated. Only the trends are of interest, since the actual magnitudes will be different for any given balance.

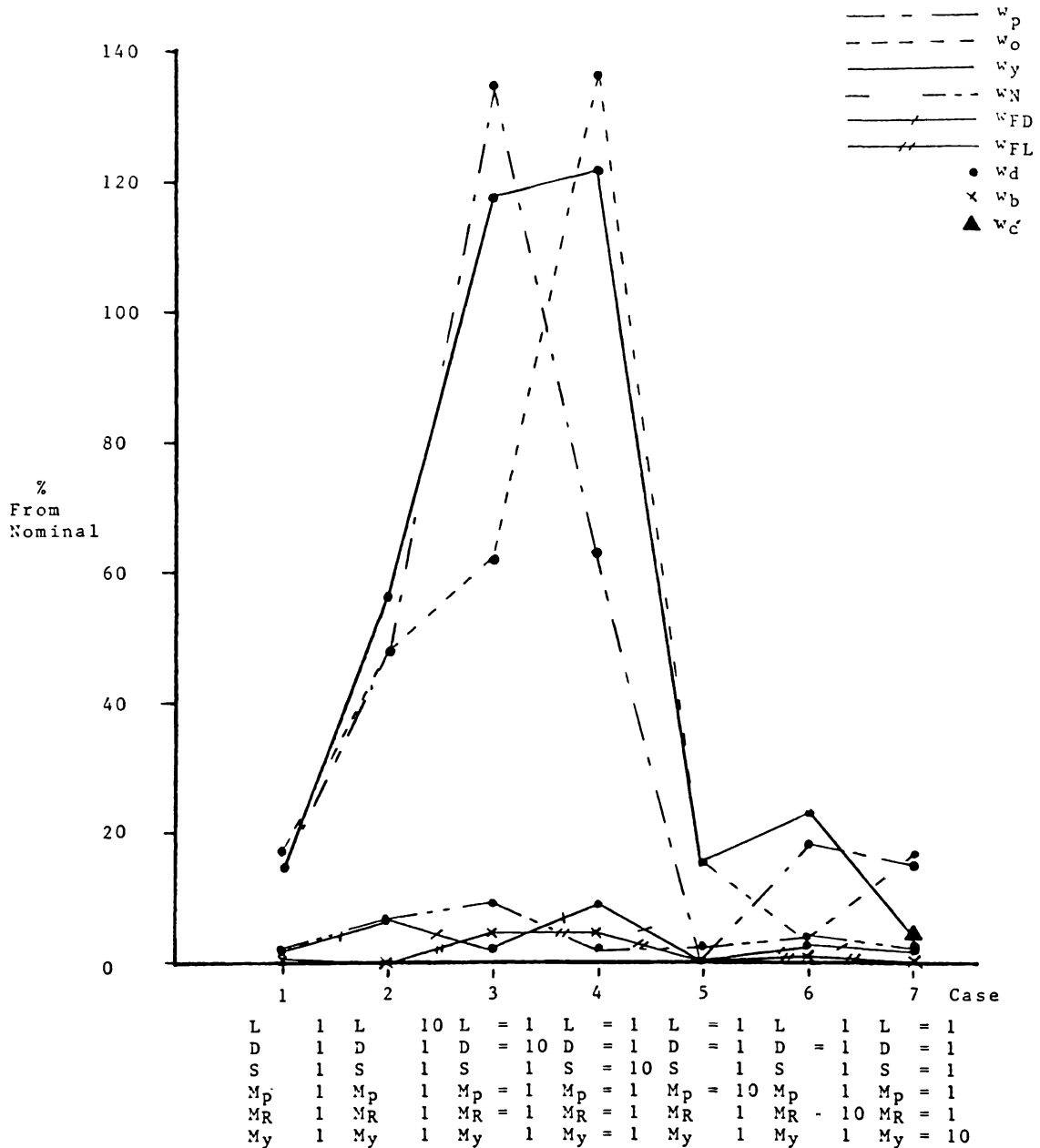


Fig. 36. % From Nominal versus Case histogram: pyramidal.

It was also found that these trends remained about the same for different signs (+/-) on the applied loads, L , D , S , M_p , M_R , and M_y .

The following observations can be made from the output data and the histogram in Figure 36:

- A: w_c and w_k have little to no major affect on any of the output uncertainties.
- B: w_c , significantly affects only the output uncertainty w_y .
- C: From Figure 36, it is seen that the moment reaction uncertainties, w_p , w_R , and w_y , are the most affected by tolerance uncertainties. On the other hand, the force reactions uncertainties, w_N , w_{FD} , and w_{FL} , have relatively small output uncertainties.
- D: w_p has the largest uncertainty in case (3) when the drag force, (D), and the linkage length tolerance uncertainty, w_d , are dominant.
- E: w_R has the largest uncertainty in case (4) when the side force, (S), and the linkage length tolerance uncertainty, w_d , are dominant.
- F: w_y has the largest uncertainty in cases (3) and (4) when the drag and side forces and the linkage length tolerance uncertainty, w_d , are dominant.
- G: w_N has the largest uncertainty in case (3) when the drag force and the linkage length tolerance uncertainty, w_d , are dominant.

- H: w_{FD} has the largest uncertainty in case (4) when the side force and the linkage length tolerance uncertainty, w_d , are dominant.
- I: w_{FL} has the largest uncertainty in cases (3) and (4) when the drag and side forces and the platform dimension, b , tolerance uncertainty, w_b , are dominant.
- J: w_b , w_d , and w_e are the most critical tolerances for all of the output uncertainties and must be as small as possible. As can be seen in Figure 36, the variance of w_d is responsible for nearly all the maximum output uncertainties.

Observation J is the most significant because a variance with any of the machined dimensions b , d , and e would have an effect on the balance's point of resolution. As was discussed in the conceptual development of the pyramidal balance (Section A), the point of resolution is the projected focal point of the pyramidal links. Consequently, it is critical that the line of action of all the applied loads intersect at this location. Any significantly large tolerances with dimensions b , d , and e would prevent this from occurring and cause higher output uncertainties. This, in turn, places an undesired emphasis on the accuracy of the balance calibration process, which is itself limited to a finite uncertainty.

CHAPTER IV
OTHER FORCE BALANCES

A. Six Component Floating Beam:

1. Concept:

A second type of six component force balance is known as the "floating beam" balance (Figure 37). A balance of this type was designed at Embry-Riddle Aeronautical University and has been used with varying degrees of success over the past seven years.

The advantages of the floating beam balance are that it is simple to construct and repair and easy to understand. Its foremost disadvantage is that a number of the output channels are coupled. Thus, the forces and moments must be separated by calibration curves and/or the simultaneous solution of the balance equilibrium equations. Also, by the nature of its configuration, the balance is prone to larger deflections than its pyramidal counterpart. In any balance, large deflections will complicate the kinematics and deteriorate the accuracy of the output.

As seen in Figure 37, the model is mounted at the top of the strut shaft. The strut shaft then extends through the test section floor and the upper block of the floating beam. Within the upper block, the shaft is held by a long, close tolerance bearing. Below the upper block, the yaw

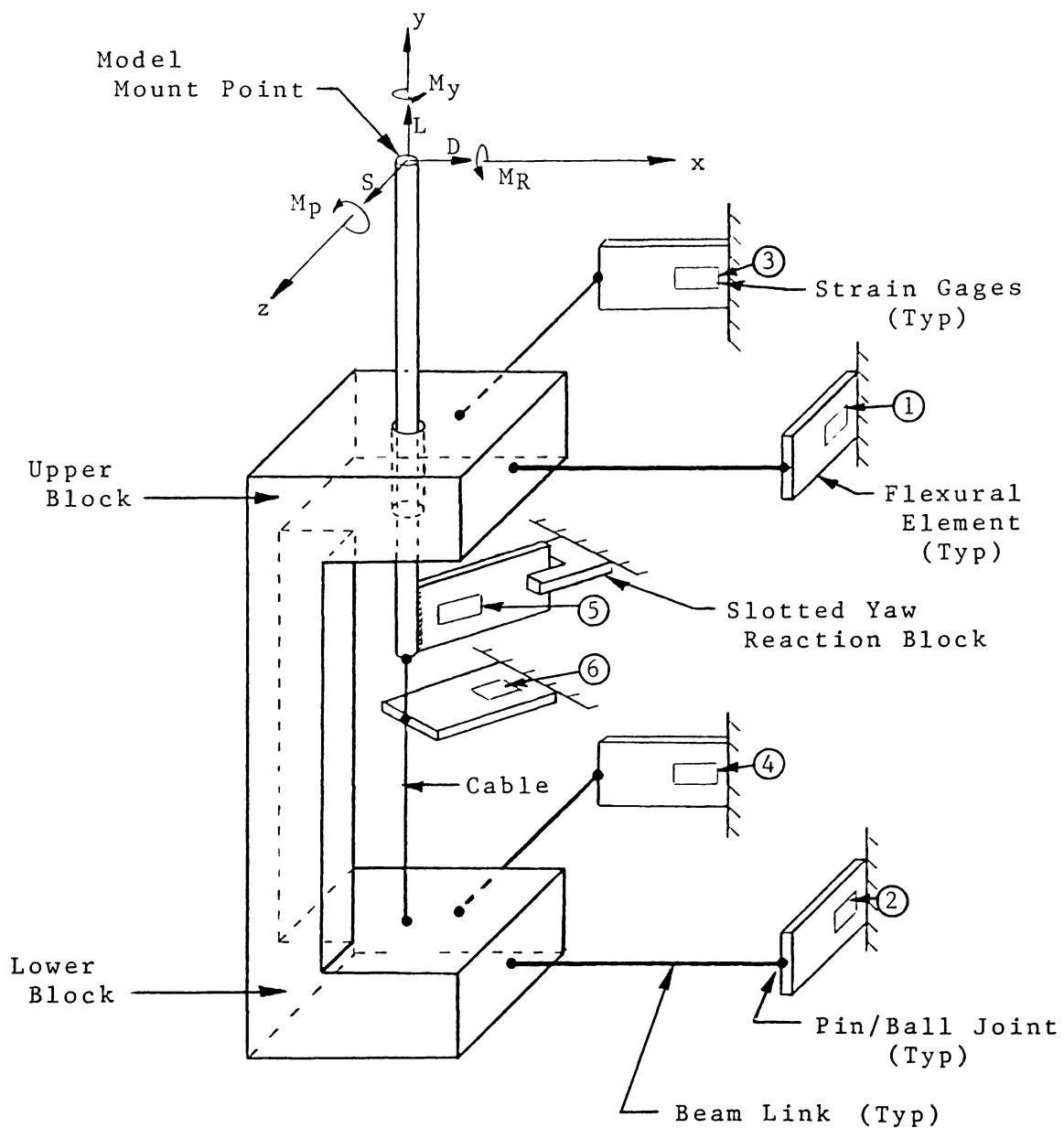


Fig. 37. Floating beam balance configuration.

flexural element (5) is attached directly to the strut shaft. Just below this, the shaft terminates into a cable. The cable then completes the load path by extending to the lower block, as shown in the figure. The reasoning behind this design will be explained in the following discussion.

Major and Minor Load Paths

To explain the concepts governing this particular balance, it is helpful to bear in mind "major" and "minor" load paths. The major load paths are those that carry a substantial portion of the given load. In general, these load paths are easily accounted for in the design analysis. On the other hand, minor load paths may be defined as those that carry only a small percentage of the load. Often, minor load paths are the cause of unexpected interactions and can give rise to difficulties in the analysis of the balance.

Now, the major and minor load paths will be reviewed for each of the applied forces and moments:

Lift

Experience has shown that, with this particular design, the lift channel is the most accurate and uncoupled. Because the shaft is prevented from vertical motion by the upper block bearing, a lift force applied to the strut shaft will lift up or push down the entire floating beam. Since the links connecting the beam to flexural elements (1), (2), (3), and (4) have ball joint ends and are normal to this major load path, no load will be transmitted to these elements (provided that the deflections are small). Furthermore, the yaw element (5) simply rides up or down in the vertical slot and registers no load as shown in Figure 37. Consequently, the entire lift load is transmitted to the lift element (6) and, except for interactions caused by system deflections, is uncoupled from the other forces.

Yaw

For the yawing moment, the major load path is the strut shaft and the yaw element. Since the shaft will tend to rotate in the upper block bearing, the yaw moment will not be transmitted to the floating beam. However, one might note that the yaw reaction at the slotted yaw block is not symmetric with respect to the balance's geometry. Thus, yaw moments are reacted by a torque and not a couple, thereby producing a secondary transverse load in the horizontal (x,z) plane. This transverse load must be balanced by the load in the linkages and elements (1) through (4). As a result, the yawing moment is not entirely uncoupled from these elements. Because of the manner in which the strain gages are mounted and because the cable below the strut shaft has negligible torsional reaction capability, the yawing moment will have no effect on the lift element (6).

Drag and Side Forces, Roll and Pitching Moments

Since the drag, side, roll and pitch forces and moments all have a similar effect on the balance system, they will be discussed together. The major load paths for these forces and moments are the strut shaft, the floating beam, and the four beam linkages. Consequently, the majority of these forces will be supported by flexural elements (1) through (4). However, each of these elements will react to a portion of each of the four forces and moments, thereby coupling them together. The forces and moments must then be separated by using calibration curves and/or the static equilibrium equations.

With the application of drag, side, roll, and pitch forces and moments, another important effect must be considered. In this situation, the floating beam will tend to rotate about a point that is a function of the stiffness of elements (1) through (4), of the applied loads, and of the length of the strut shaft. Therefore, the rotation point will shift up or down by a slight amount depending on the particular test being conducted. Since it would be ideal to locate the lift flexural element at the rotation point, it is seen that the best design can only locate the element at a general location relative to the particular testing that is anticipated during the life of the balance. So in this subtle way, the balance can be tailored towards a specific type of testing. The reason why it is desirable to have the lift element at the rotation point is to minimize or prevent interactions caused by the drag, side, roll, and pitch forces and moments. When the lift element is located exactly at the rotation point, it will not be affected by any of the applied forces or moments (except for the lift, of course). But when there is a difference between the locations, the element will be placed in slight tension or compression. Since the axial stiffness of the flexural element is much greater than its bending stiffness, this tension or compression has a negligible effect on the lift data itself. However, the minor load path created by the difference can have a significant effect on the bending of elements (1) through (4) because a load will always travel

through the stiffest path. Now it becomes clear as to the importance of the cable. A taut cable is easily deflected a small amount at or near its midspan since it offers little resistance to a transverse load. Because of this, the cable can reduce the magnitude of the coupling caused by the shifting of the rotation point.

A second significant consequence of the floating beam rotation is the tendency for the yaw beam to bind in the slot on the yaw reaction block. This again creates a minor load path that will have an effect on all the readings, with the exception of the lift. Even without any rotation, this reaction will still exist and must be accounted for.

The net result of the interactions described above is that a comprehensive set of calibration curves must be developed because it would be nearly impossible to analytically determine the extent of the coupling. In some ways, this is true for all wind tunnel force balances. But the problem can be more pronounced for a balance that must overcome both the inherent coupling and the deflection coupling as opposed to a balance that has interactions caused only by deflections.

2. Static Analysis:

The static equations of equilibrium for the floating beam balance will now be derived.

The general free body diagram of the floating beam is shown in Figure 38:

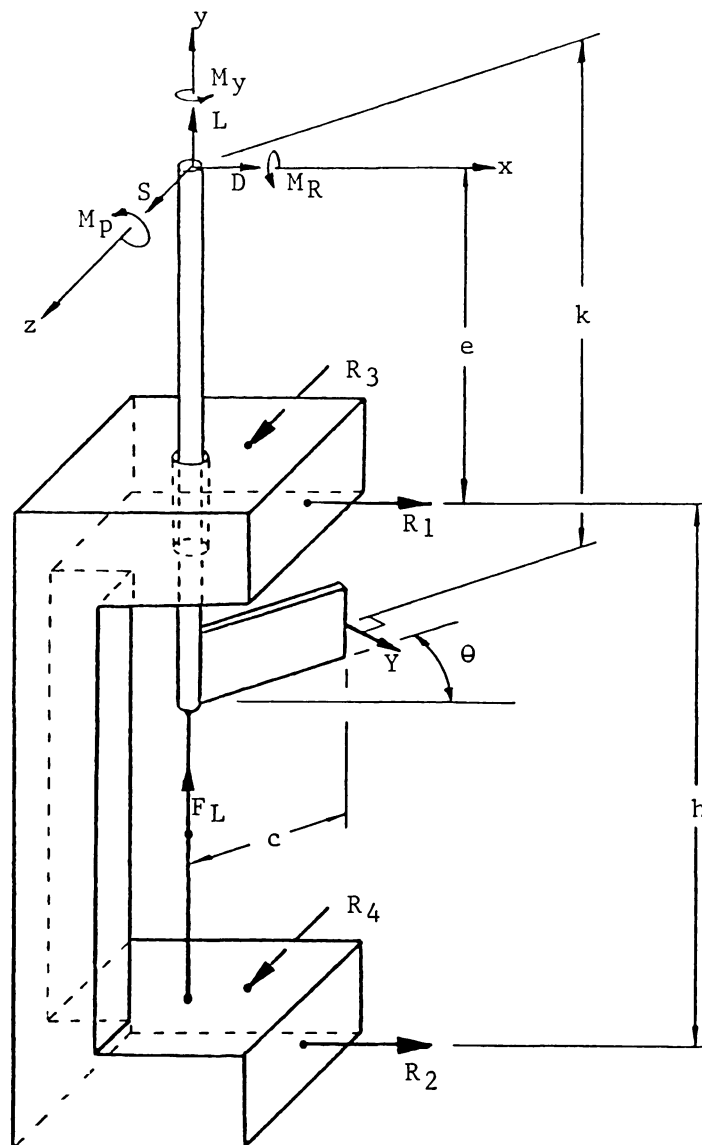


Fig. 38. Floating beam free body diagram.

From Figure 38, summing the forces in the x-direction:

$$D + R_1 + R_2 + Y \sin \theta = 0.0 \quad 4.1$$

Summing the forces in the y-direction:

$$L = - F_L \quad 4.2$$

Thus, the lift is separate and uncoupled from the other reactions.

Summing of the forces in the z-direction:

$$S + R_3 + R_4 + Y\cos\theta = 0.0 \quad 4.3$$

Summing of the moments about the x-axis:

$$M_R - R_3e - Yk\cos\theta - R_4(h + e) = 0.0 \quad 4.4$$

Summing the moments about the y-axis:

$$M_y = Yc \quad \text{or} \quad Y = M_y/c \quad 4.5$$

The yaw reaction itself is separate and uncoupled from the other reactions; but, it will be seen that the yaw does affect some of the other reactions.

Summing the moments about the z-axis:

$$M_p + R_1e + Yk\sin\theta + R_2(h + e) = 0.0 \quad 4.6$$

Now, solving equations 4.1, 4.3, 4.4, and 4.6, for R_1 through R_4 :

$$R_1 + R_2 = -D - (M_y\sin\theta)/c \quad 4.7$$

$$M_p + (M_yk\sin\theta)/c + (R_1 + R_2)e + R_2h = 0.0 \quad 4.8$$

Substituting 4.7 into 4.8 and rearrange to obtain:

$$R_1 = -D(1 + e/h) - (M_y\sin\theta)(1 + e/h - k/h)/c + M_p/h \quad 4.9$$

$$R_2 = \{ De + (M_y\sin\theta)(e - k)/c - M_p \} / h \quad 4.10$$

Similarly,

$$R_3 + R_4 = -S - (M_y\cos\theta)/c \quad 4.11$$

$$M_R - (M_yk\cos\theta)/c - (R_3 + R_4)e - R_4h = 0.0 \quad 4.12$$

Substitute 4.11 into 4.12 and rearrange to get:

$$R_3 = -S(1 + e/h) - (M_y\cos\theta)(1 + e/h - k/h)/c - M_R/h \quad 4.13$$

$$R_4 = \{ Se + (M_y\cos\theta)(e - k)/c + M_R \} / h \quad 4.14$$

It can now be seen that R_1 through R_4 are each inherently a function of three forces or moments. R_1 and R_2 are both a function of drag, yaw, and pitch. R_3 and R_4 are influenced by the side force, yaw, and roll. In practice, R_1 through R_4 are known from the strain gages and prior calibrations. The unknown forces are found by direct substitution into equations 4.1, 4.3, 4.4, and 4.6.

These equations become:

$$D = - (R_1 + R_2) - Y \sin \theta \quad 4.15$$

$$S = - (R_3 + R_4) - Y \cos \theta \quad 4.16$$

$$M_p = - (R_1 + R_2)e - R_2 h - Y k \sin \theta \quad 4.17$$

$$M_R = (R_3 + R_4)e + R_4 h + Y k \cos \theta \quad 4.18$$

Again, note the influence of yaw in each of the above equations.

By the nature of the configuration, R_2 will tend to be opposite to R_1 , as will R_4 to R_3 . Therefore, in each of the above equations there will be a difference between two large forces. Because of electrical considerations with the strain gages, there could be a significant amount of error in this difference. This error is, of course, in addition to what may exist from deflections. It is for these reasons that coupling is generally undesirable in the design of a force balance.

The effect of the yaw in equations 4.15, 4.16, 4.17, and 4.18 could be eliminated by a slight design modification: make the yaw reaction a symmetric one with respect to the balance's geometry as shown in Figure 39:

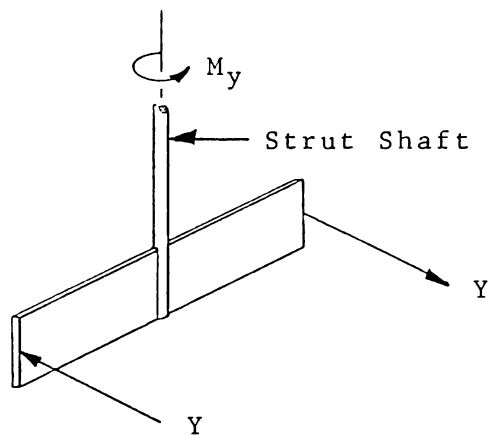


Fig. 39. Yaw flexural element

This configuration was previously used with the pyramidal balance design.

B. Three Component Strain Gaged Strut:

1. Concept:

The configuration of a three component strain gaged balance used in the Embry-Riddle wind tunnel laboratory appears in Figure 40:

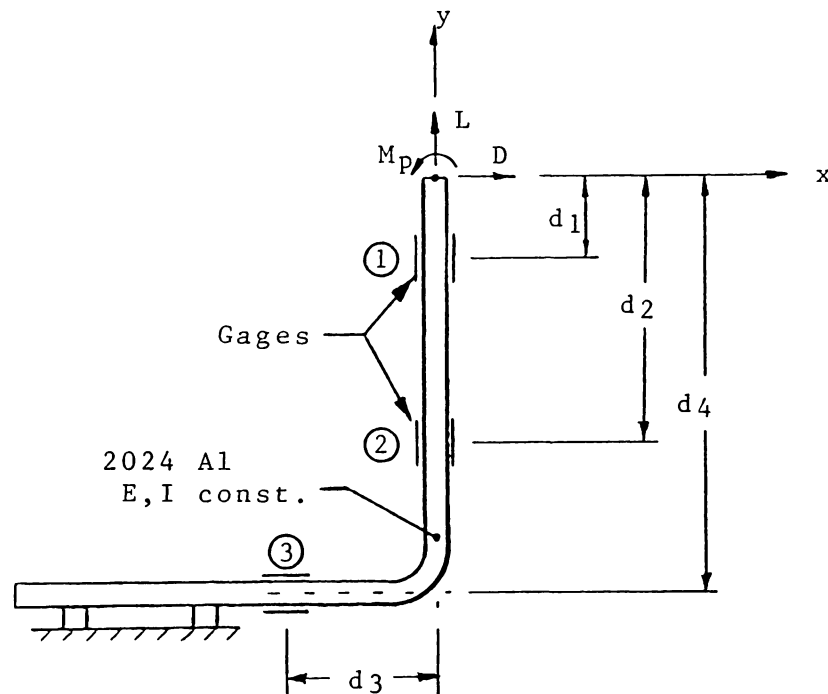


Fig. 40. Three component strain gaged strut configuration.

The foundation of this concept is the manner in which the strain gages are placed on the strut and how they are used by the strain measurement system. In Figure 40, one will notice that there are gages on both sides of locations (1), (2), and (3). With this particular balance, there is only one gage on each side of the aluminum bar; there could just as well be two.

There are two advantages to using multiple gages at a given balance location as opposed to only one:

1. By using a Wheatstone bridge, multiple gages can increase the electrical output, thereby increasing the accuracy of the balance.
2. Again, through the use of a Wheatstone bridge, some of the forces can be decoupled.

At location (1), the gages are affected by two moments (M_p and Dd_1) and an axial force (L). If only one gage were used, all three of the loads would be a part of the final strain readout. But with two or four gages properly placed in a Wheatstone bridge, the strain due to the axial force (L) can be canceled out. Thus, only the strain from the two moments is measured. Consequently, by electrical means, the degree of coupling (to be discussed in Chapter V) is reduced. The same also holds true for locations (2) and (3). In practice, because of the amount of coupling present, this balance relies heavily on calibration equations for the final output data.

2. Static Analysis:

One of the advantages of this balance is that the static analysis is elementary. It is easily shown that the bending moments at locations (1), (2), and (3) are:

$$M_1 = M_p - Dd_1 \quad 4.19$$

$$M_2 = M_p - Dd_2 \quad 4.20$$

$$M_3 = M_p + Ld_3 - Dd_4 \quad 4.21$$

These are the moments that will induce the strain indicated

on the strain gages.

3. Uncertainty Analysis:

The uncertainty of the above moments, with respect to the nominal locations of the strain gages at points (1), (2), and (3), can be found by the analysis technique previously used on the pyramidal balance. The fundamental point remains the same here as it did for the pyramidal system. The uncertainties found in this analysis are useful in determining how accurately the strain gages need to be located. For M_1 from equation 4.19, the partial derivative is:

$$\partial M_1 / \partial d_1 = - D$$

Therefore,

$$w_{M1} = (D^2 w_{d1}^2)^{1/2}$$

$$w_{M1} = D w_{d1} \quad 4.22$$

For M_2 from equation 4.20:

$$\partial M_2 / \partial d_2 = - D$$

$$w_{M2} = D w_{d2} \quad 4.23$$

For M_3 from equation 4.21:

$$\partial M_3 / \partial d_3 = L \quad \text{and} \quad \partial M_3 / \partial d_4 = - D$$

$$w_{M3} = (L^2 w_{d3}^2 + D^2 w_{d4}^2)^{1/2} \quad 4.24$$

Appendix B. includes a numerical example of the above.

Uncertainty Assessment - Three Component Strain Gaged Strut

In the same manner as the pyramidal balance, a series of cases with varying loads and tolerances are considered by the variation of parameters method. With the assistance of a computer, the following cases were considered:

1. All loads = 1.0 lb or in-lb
2. L = 10 lb All other loads = 1.0 lb or in-lb
3. D = 10 lb " "
4. M_p = 10 in-lb " "

Under each load case, the dimensional tolerances were individually varied from 0.001" to 0.1" in five subcases:

- a: All tolerances = 0.001 in
- b: w_{d1} = 0.1 in All other tolerances = 0.001 in
- d: w_{d2} = 0.1 in " "
- e: w_{d3} = 0.1 in " "
- f: w_{d4} = 0.1 in " "

The output uncertainties that are of the most interest are the maxima and their associated tolerance subcases. This information can be conveniently graphed on a histogram as maximum % from nominal versus case (see Figure 41). As with the pyramidal balance, each point plotted on the graph represents the maximum uncertainty variance from nominal for a given load case. In the legend, the subcase tolerance that caused the maximum variance is indicated. Again, only the trends are significant since the actual magnitudes will be different for any given balance.

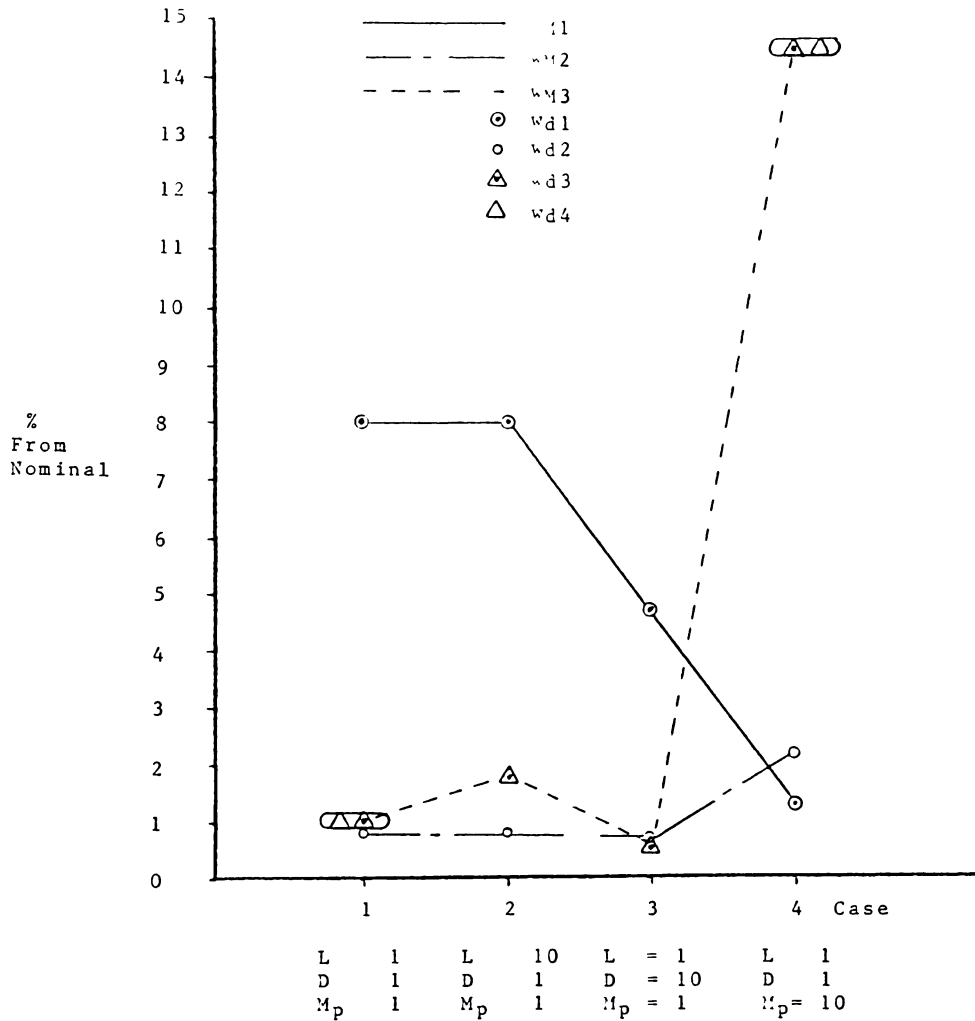


Fig. 41. % From Nominal versus Case histogram: strut.

Observations from the histogram (Figure 41):

- A: No single dimension is dominant, as was the case with the pyramidal balance.
- B: The worst case uncertainty occurrence is with the bending moment at point 3 when the pitch moment is dominant.

Observation (A) was expected. The histogram simply indicates that the worst uncertainties of moments M_1 and M_2 are driven by the uncertainty of their related dimensions,

d_1 and d_2 , respectively. Likewise, the uncertainty of moment M_3 is a function of the uncertainties of d_3 and d_4 . It is important to remember that the trends shown on the histogram for w_{M1} and w_{M2} are independent of the lift. The reason for a large w_{M1} in cases 1 and 2 is that the nominal moment caused by D and M_p is relatively small; so when w_{d1} is varied, the percent difference from nominal will be large. The fact that the lift is large in case 2 plays no role in this difference from nominal. The same is true for w_{M2} in cases 1 and 2.

CHAPTER V

CLASSIFICATION OF FORCE BALANCES

A. Classification Method:

Nearly all of the sources agree that wind tunnel balances can be categorized as either being internal or external. Unfortunately, the consensus ends there. The vast majority of published literature discuss only a specific application or part of a given balance. Most force measurement systems are designed and built for a special purpose. Balances are often used only within a certain aerodynamic regime (such as subsonic or supersonic) at ambient or cryogenic temperatures. As a result, most of the available literature will reflect such conditions. There is an apparent lack of a definition of balances based on their kinematical functions. Similarly, there is very little in the literature that deals with the analysis of these functions. The reasons for these are two-fold. First, the detailed kinematic and elastic effects within a force balance (especially with force and moment interactions) are very complex and go far beyond the simple equations of statics. Secondly, because the demand for balances is small, there are only a few force balance manufacturers. Manufacturers who have much of the detailed information often consider it proprietary. This is particularly evident

for balances that operate on mechanical (as opposed to magnetic suspension) and/or elastic principles. Of course, this encompasses most modern balances.

With regard to classifications, Pope subdivides external balances into four very specific types: wire, platform, yoke, and pyramidal. On the other hand, Gorlin subdivides external balances into only two very general types: balances that have coupled interactions between the readout channels and balances that have uncoupled, independent readout channels. Clearly, with the first classification criterion being so specific, it may not be possible to apply it to some of the nonstandard balance designs. Similarly, the other criterion is so general that it fails to provide an accurate mechanical description of the device in question.

For example, Gorlin's method would place the pyramidal balance in one category since it can separate all of the force and moment components into corresponding reactions. On the other hand, it would place both the six component floating beam balance and the three component strain gaged strut balance in the second category since both balances have coupled reactions. This is hardly an adequate description of these latter balances because, from a mechanical view, they are greatly different. The floating beam is composed of a number of linkages, nuts, bolts, and associated hardware that can give rise to tolerance and hysteresis problems. Since these mechanical characteristics are not present on the simple strain gaged strut, there is a

considerable difference between these two force measurement systems that needs to be accounted for.

An alternative method for classifying external balances is to entirely disregard Pope's approach and expand upon Gorlin's. This can be accomplished by first defining the degree, (n), to which a given balance is coupled:

n = the average number of applied forces or moments that the balance is measuring that influence each readout channel.

Examples on how the degree of coupling is found for a given force measurement system is included in Appendix C.

This definition will incorporate two important characteristics that are overlooked by other classification methods. The first is the actual number of load cells, flexural elements, or transducers (whatever type they may be) that are affected by an applied load or moment. The second is the number of components or degrees of freedom that the balance is designed to measure (i.e. 3, 4, 6-component, etc.). By including these characteristics in this classification method, virtually all of the external mechanical and/or elastic force balance systems can be compared, regardless of their intended purpose.

The degree of coupling is only one of two important parameters that are used in this classification method. The second involves the number of linkages and pivots that are present in a given balance design. A balance that is mechanically complex (as manifested by the number of joints,

links, and hinges) can experience significantly more tolerance and hysteresis problems than a balance that is of a more singular design. This is an important factor that must be accounted for. With this method, no attempt is made here to account for the magnitude of these tolerances, only to acknowledge their presence. It can be seen in Appendix C that two given balances may have the same degree of coupling but are radically different from each other in terms of mechanical complexity. Therefore, the hardware parameter, (p), is defined to be:

p = the average number of joints, pivots, and mechanical interfaces that any given load may encounter from its origin enroute to the measuring devices (load cells, flexural elements, or strain gages)

Again, the application of this parameter is included in Appendix C.

Ultimately, both of these parameters are placed in a table that contains the (n) and (p) of other force balances. From this table, general comparisons can be made between the different balance designs.

B. Outline of Method:

The following is an outline of how to apply this method.

Degree of Coupling, (n):

1. The static equations of equilibrium for the balance are found. These are solved for the measured reactions in terms of the applied forces and moments (lift, drag, or

side; pitch, roll, or yaw). The measured reactions are those read via the load cells, flexural elements, or stain gages.

2. Count the number of applied forces and/or moments that are present for each measured reaction. The coupling number, (c), is then found by summing the number of applied forces and/or moments that are present for all of the measured reactions.

3. The degree of coupling, n, is defined as the quotient of the coupling number, c, and the total number of measured reactions that are present on the balance. This yields the average number of forces and/or moments per measured reaction as stated in the definition of n.

Hardware Parameter, (p):

4. The hardware parameter is found by considering, one at a time, each individually applied force or moment. Follow the load path and count all the links, joints, pivots, mechanical interfaces, and any other hardware that may have rotational or translational tolerances. After this has been done for all the loads to be measured, obtain a sum of affected links, pivots, and mechanical interfaces. The hardware parameter is defined as the quotient of this sum and the total number of forces and moments that the balance system is designed to measure.

5. Classify the balance by placing (n) and (p) in the following table with the results of the other force measurement systems.

6. Note the relative magnitudes of (n) and (p) in the table as compared with other typical balance designs. An assessment can then be made as to the systems general weaknesses and strengths. Further comments with regard to the magnitude of (n) and (p) are made in Chapter VI.

This classification procedure is more detailed and comprehensive than those presented by the common references. It is recognized that this method may be cumbersome but it does reflect the complexity and to some extent, the accuracy of any particular balance. In the design and development of a particular force measurement system, there is interest in knowing how that system compares with other designs. The method outlined here satisfies that interest.

To understand exactly how this classification method is applied to a force measurement system, a number of examples have been worked out and are presented in Appendix C. The following table is a summary of the results from these examples:

EXAMPLE	n	p
A: 2 component strain gaged strut	2	1
B: 3 component strain gaged strut	2.333	1
C: 6 component floating beam	2.333	5
D: 3 component pyramidal	1	13.7
E: 6 component pyramidal	1	21.7
F: 3 component smoke tunnel	2.667	3.33
G: 6 component platform	2.83	6.5
H: 6 component yoke	2	4.83

CHAPTER VI
CONCLUSIONS

A. General:

The last ninety years of aviation history have been marked by significant breakthroughs as a result of wind tunnels and their associated force measurement systems. In this thesis, a few of these systems were discussed in detail.

Some of the more important aspects that apply to all balances are those of coupling and deflections. Generally, for an uncoupled external balance (such as the pyramidal configuration) high confidence in the measured data can be achieved without a large dependence on calibration. Conversely, the complexity of the linkages and levers (all machined to close tolerances) required to uncouple the loads determine the cost of such a balance. This cost can be high when compared with alternate configurations. External balances that are highly coupled tend to be less expensive as well as easier to construct and understand. However, their output data validity relies almost entirely on the accuracy of the calibration thus producing measured results with larger uncertainty margins.

Deflections of components within a force measurement system can be significant because they give rise to

secondary coupling effects that are not detectable from kinematic evaluations. These mandate that all balances be calibrated including those that are considered to be entirely uncoupled. Ideally, to prevent angle of attack, yaw, and roll problems, a given balance should have deflections that are as small as practicable. When strain is the net variable of the output, a compromise exists in that small deflections result in small strains. Consequently, the output of the strain measurement system may be subject to nonlinearity problems. It has been shown that for values less than several hundred microstrain, the modulus of elasticity for most common balance material (aluminum, steel, etc.) is non-linear [11]. This, of course, would cause output errors since the entire calibration process is based upon the linear assumptions of a Hookian type material (stress linearly related to strain).

B. Balance Systems:

With the three and six component pyramidal balance configurations considered here, it has been shown (under the assumptions made) that all the measured reactions are statically uncoupled and independent of each other. As a result the balance is mechanically more complex and would be more expensive to build than other conceivable designs. The uncertainty of the output reactions (with reasonable construction tolerances) has been shown to be relatively small. With regard to uncertainty, the most critical dimensions on the balance are the length of the pyramidal

links, d , the half-width of the platform, b , and the length of the model attachment strut, e . All these dimensions should be machined to the closest possible tolerance to provide maximum accuracy of the output reactions.

The six component floating beam balance has several advantages over the pyramidal design. It is easy to construct and, on a comparative scale, as much as one fiftieth as expensive as a commercially made pyramidal balance for the same size tunnel. Also, it is an easy balance to understand conceptually. Therefore, repairs and modifications can be made to this balance with minimal difficulties. The drawbacks of this system are the inherent degree of coupling, numerous areas where hardware tolerances are present (like the pyramidal), and the relatively large system deflections.

Another balance system that shares many characteristics with the floating beam is the three component strain gaged strut. It is easy to construct as well as repair and modify. This design, though, is highly coupled and has very small gage readouts that may give rise to some of the difficulties previously mentioned with low strains.

C. Classification:

Wind tunnel balances have been classified by a new method based upon two parameters: the degree of coupling, n , and the hardware parameter, p . This new method is more detailed and encompassing than the balance classifications used by references [5] and [6]. It is applicable to nearly

any balance configuration conceivable, regardless of the number of components it has as part of its design. One difficulty of this method is that it requires a nearly complete understanding of the balance in question. The method is not applicable when the load paths and interactions have not been fully defined.

The degree of coupling, n , is defined as the average number of applied forces or moments that the balance is measuring which affect each readout channel. Note that n is dependent only on a theoretical static analysis when in fact, due to deflections, the degree of coupling could be higher.

The hardware parameter, p , is defined as the average number of joints, pivots and mechanical interfaces that any given load path may encounter enroute to the measuring devices. Typically, as the hardware parameter for an external balance rises, so do the cost and tolerance uncertainties.

The degree of coupling and hardware parameter have been found for the following balances featured in this thesis:

Three component pyramidal:	$n = 1.0$	$p = 13.7$
Six component pyramidal:	$n = 1.0$	$p = 21.7$
Six component floating beam:	$n = 2.333$	$p = 5.0$
Three component strain gaged strut:	$n = 2.333$	$p = 1.0$

D. Recommendations:

It is recommended that future investigations include:

- a) a determination of the effects of deflection on the pyramidal force balance,
- b) an investigation of the uncertainties of low strains with the three component strain gaged strut, and
- c) a redesign and rebuilding of a new six component floating beam balance.

The foundation for a pyramidal balance deflection analysis has been laid out here since many of the system's loads were determined in Section B of Chapter III.

Possible points of interest would include determining which component deflection would cause the greatest error or coupling and what the output uncertainties due to a combination of deflections might be. It is suspected that axial deflections of any of the pyramidal linkages and/or bending deflections of the model mount strut may prove to be some of the more critical deflections. This suspicion is based upon the uncertainty analysis presented herein which demonstrated that any dimensional change affecting the point of resolution will cause significant uncertainties in the output.

A more complete investigation should be made of the uncertainties caused by low strain levels on the existing three component strain gaged strut. This analysis should be at least two-fold. One, determine what the lowest

permissible strain levels should be such that the uncertainties of the electrical equipment will have only a minimal effect. Second, the effect of a non-linear modulus of elasticity on the calibration equations should be investigated more thoroughly.

Finally, the six component floating beam balance should be redesigned and rebuilt. The primary objectives in the redesign effort should be to reduce the system's deflections (without allowing the readout strains to become too low) and to eliminate the yaw couple interactions described in Section A of Chapter IV. The motivation behind this effort is that the floating beam is an "in house" balance that can be easily constructed and modified with minimum tooling and facilities.

APPENDIX A

Example of Numerical Uncertainty: Pyramidal Balance

It is instructive to make a numerical evaluation of the uncertainty equations derived in Chapter III. Consider the following set of typical values for a small wind tunnel:

L = 30 lb	$M_p = 5 \text{ in-lb}$
D = 15 lb	$M_R = 1 \text{ in-lb}$
S = 3 lb	$M_y = 2 \text{ in-lb}$

and

a = 6 in	d = 11.66 in
b = 6 in	e = 8 in
c = 2 in	h = 8 in
c' = 4 in	k = 10 in

where a and h are determined from the geometric relations:

$$d = [2a^2 + h^2]^{1/2} \quad \text{A1}$$

$$e = bh/a \quad \text{A2}$$

Equations A1 and A2 were found in Section B of Chapter III.

It is assumed that all machining tolerances can be held to within:

$$w = \pm 0.005 \text{ in.}$$

Therefore, the tolerance uncertainties for the "machined" dimensions b, c, c', d, e, and k are:

$$w_b = w_c = w_{c'} = w_d = w_e = w_k = \pm 0.005 \text{ in.}$$

The "assembly" dimensions, a and h, and their uncertainties must be determined from equations A1 and A2. Machined dimensions can be considered as those associated with individual parts and pieces of the balance (links, platform,

etc.). The assembly dimensions are those that are present on the assembled balance system. Therefore, the uncertainties that pertain to the assembly dimensions are dependent upon those of the machined dimensions.

Rearranging equations A1 and A2 gives:

$$a = d[2 + (e/b)^2]^{-1/2}$$

$$h = d[1 + 2(b/e)^2]^{-1/2}$$

Applying equation 3.89 for the uncertainty yields:

$$w_a = d(e/b)^2[(w_b/b)^2/X^3 + (w_d/d)^2(b/e)^4/X + (w_e/e)^2/X^3]^{1/2} \quad A3$$

$$w_h = d(b/e)^2[4(w_b/b)^2/Z^3 + (w_d/d)^2(e/b)^4/Z + 4(w_e/e)^2/Z^3]^{1/2} \quad A4$$

Where, $X = 2 + (e/b)^2$
 $Z = 1 + 2(b/e)^2$

Substituting into equations A3 and A4 gives:

$$w_a = \pm 0.004 \text{ in.}$$

$$w_h = \pm 0.006 \text{ in.}$$

The nominal values of the moment reactions are found to be:

Pitch: $P = M_p/k = 0.5 \text{ lb}$
 Roll: $R = M_R/k = 0.1 \text{ lb}$
 Yaw: $Y = M_y/c' = 0.5 \text{ lb}$

Then, by the use of equations 3.90 through 3.99 and 3.104 through 3.108 and 3.113, the following results are obtained:

$$\begin{aligned} w_p &= \pm 0.0162 \text{ lb} \approx 3.2 \% \text{ from nominal} \\ w_R &= \pm 0.0116 \text{ lb} \approx 11.6 \% \quad " \\ w_y &= \pm 0.0400 \text{ lb} \approx 8.0 \% \quad " \\ w_N &= \pm 0.0164 \text{ lb} \approx 0.5 \% \quad " \\ w_{FD} &= \pm 0.0229 \text{ lb} \approx 0.2 \% \quad " \\ w_{FL} &= \pm 0.0060 \text{ lb} \approx 0 \% \quad " \end{aligned}$$

APPENDIX B

Example of Numerical Uncertainty:

Three Component Strain Gaged Strut

Consider the following typical loads and dimensions for this balance:

$$\begin{array}{ll} L = 10 \text{ lb} & d_1 = 2.25 \text{ in} \\ D = 5 \text{ lb} & d_2 = 14.5 \text{ in} \\ M_p = - 0.5 \text{ in-lb} & d_3 = 7.0 \text{ in} \\ & d_4 = 17.69 \text{ in} \end{array}$$

It is reasonable to say that the careful application by hand of the strain gages will yield dimensional tolerances of:

$$w_{d1} = w_{d2} = w_{d3} = w_{d4} = \pm 1/16 \text{ in} = \pm 0.063 \text{ in}$$

From equations 4.19, 4.20, and 4.21, the nominal values are:

$$M_1 = - 11.75 \text{ in-lb}$$

$$M_2 = - 73.0 \text{ in-lb}$$

$$M_3 = - 19.0 \text{ in-lb}$$

Thus, by equations 4.22, 4.23, and 4.24:

$$w_{M1} = \pm 0.315 \text{ in-lb} \approx 2.7 \% \text{ from nominal}$$

$$w_{M2} = \pm 0.313 \text{ in-lb} \approx 0 \% \quad "$$

$$w_{M3} = \pm 0.704 \text{ in-lb} \approx 3.7 \% \quad "$$

APPENDIX C

Examples of Classification

Using the method outlined in Chapter V, a number of balances are classified in the following examples. The results of these examples are summarized at the end of Chapter V.

Example A: Two component strain gaged strut

As the first example, the classification parameters for a simple two component strain gaged strut will be found.

1.

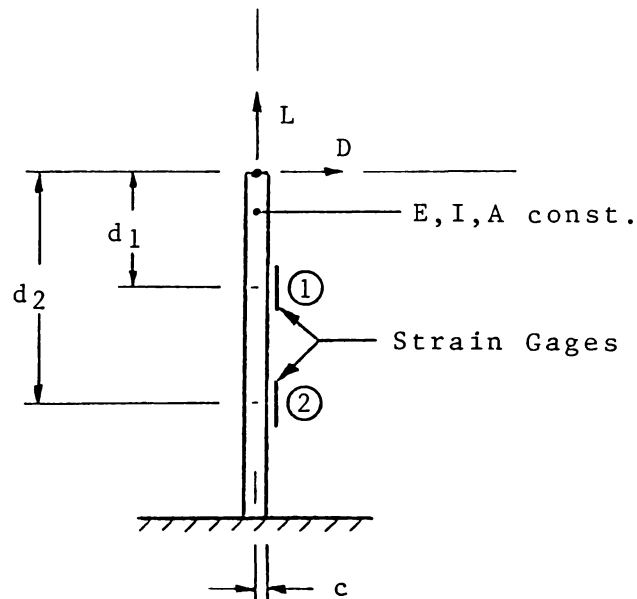


Fig. 42. Two component strain gaged strut.

In this case, the measured reactions are the strains at locations (1) and (2). Thus, the total strain at (1), ϵ_1 , is

given by the sum of the strains caused by the lift and drag forces:

$$\epsilon_1 = \epsilon_L + \epsilon_D \quad C1$$

Assuming that the material obeys Hooks law, the strain is a linear function of the stress, σ :

$$\epsilon_1 = \sigma_L/E + \sigma_D/E \quad C2$$

Where from the basic solid mechanics of materials:

$$\sigma_L = L/A \quad \text{and} \quad \sigma_D = - Dd_1c/I \quad (\text{in compression})$$

Thus, for step 1 of the methods outline (Section B, Chapter V):

$$\epsilon_1 = L/(EA) - Dd_1c/(EI) \quad C3$$

and

$$\epsilon_2 = L/(EA) - Dd_2c/(EI) \quad C4$$

These two equations can now be simultaneously solved for any combination of lift and drag.

2. In equations C3 and C4: note that reaction one, ϵ_1 , is a function of two of the applied forces, L and D. The same is also true of reaction two, ϵ_2 .

Thus,

ϵ_1 --> function of 2 applied loads

ϵ_2 --> function of 2 applied loads

$$\Rightarrow c = 2 + 2$$

$$\underline{c = 4}$$

3. Now, find the degree of coupling, n:

Since there are two measured reactions, ϵ_1 and ϵ_2 :

$$n = c/2 \quad \Rightarrow \underline{n = 2}$$

4. For this example, the hardware parameter, (p), is straightforward. The only joint or pivot present would be

at the top of the strut where the forces are applied. This interface is always present for all balances.

Apply each load separately and count the number of pivots, joints, and connections that will be affected by the load path.

Lift:

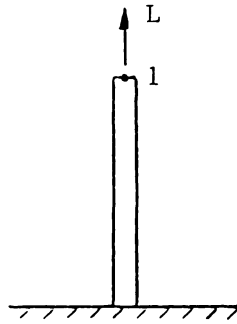


Fig. 43. Lift applied to two component strut.

In Figure 43, the load path passes through only one pivot, at location (1).

Drag:

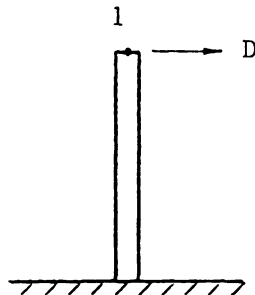


Fig. 44. Drag applied to two component strut.

In Figure 44, the load path again only passes through one pivot, at location (1).

Thus, the total sum of pivots affected is: $s = 1 + 1 = 2$

Since this is a two component system, the hardware parameter is:

$$p = s/2$$

$$\underline{p = 1}$$

Example B: Three component strain gaged strut

In this example, the parameters for Embry-Riddle's three component strain gaged strut balance shown in Figure 40 are found.

1. The measured reactions, for this balance, are the total moments at locations (1), (2), and (3), as shown in Chapter IV.

Thus,

$$M_1 = M_p - Dd_1$$

$$M_2 = M_p - Dd_2$$

$$M_3 = M_p + Ld_3 - Dd_4$$

Where M_1 , M_2 , and M_3 are known through the decoupling described in Chapter IV.

2. Therefore,

$$M_1 \text{ --> function of 2 applied loads}$$

$$M_2 \text{ --> " 2 "}$$

$$M_3 \text{ --> " 3 "}$$

$$\text{==> } c = 2 + 2 + 3 = 7$$

3. Since there are three measured reactions:

$$n = c/3$$

$$\underline{n = 2.333}$$

4. Like Example A, the only hardware tolerance problem could be at the pivot at the top of the strut where the forces and moments are applied.

Therefore,

Lift: effects 1 pivot in the load path

Drag: " 1 "

Pitch: " 1 "

$$\Rightarrow s = 1 + 1 + 1 = 3$$

Since this is a three component balance,

$$p = s/3$$

$$\underline{p = 1}$$

Example C: Six component floating beam

For the classification parameters of the floating beam balance, refer to the static analysis for the equations of the measured reactions (Section A, Chapter IV).

1. The measured reactions are given by equations 4.2, 4.5, 4.9, 4.10, 4.13, and 4.14.
2. Thus, the coupling number, c is:

F_L = function of 1 applied load

Y = " 1 "

R_1 = " 3 "

R_2 = " 3 "

R_3 = " 3 "

R_4 = " 3 "

$$\Rightarrow c = 1 + 1 + 3 + 3 + 3 + 3 = 14$$

3. Since there are six measured reactions, the degree of coupling is:

$$n = c/6$$

$$\underline{n = 2.333}$$

Note that this is the same degree of coupling as found

with the strain gaged strut in Example B.

In the static analysis in Chapter IV, a design change is noted that would eliminate the yaw in the equations for R_1 through R_4 . With this change, the degree of coupling could be reduced to: $n = 1.667$

4. To find the hardware parameter for the floating beam balance, all of the joints, connections, pivots, etc. that may have a bearing on tolerance problems are sequentially numbered on Figure 45 on the next page.

Counting the places that have an affect on each individual load path:

Lift:	1, 8, 9, 10	-->	function of 4 applied loads
Drag:	1, 2, 5, 6, 13, 14	-->	" 6 "
Side:	1, 2, 3, 4, 11, 12	-->	" 6 "
M_R :	1, 2, 3, 4, 11, 12	-->	" 6 "
M_y :	1, 7	-->	" 2 "
M_p :	1, 2, 5, 6, 13, 14	-->	" 6 "

$$\Rightarrow s = 4 + 6 + 6 + 6 + 2 + 6 = 30$$

For a six component balance: $p = s/6$

$$\underline{p = 5.0}$$

Note that the location 7 was not included in the drag, side, M_R , and M_p load paths because any tolerance here would only help to decouple these reactions. If the design change on the yaw flexural element noted in Chapter IV were implemented, another yaw reaction block would be necessary. Consequently, the value for the hardware parameter, p , would rise.

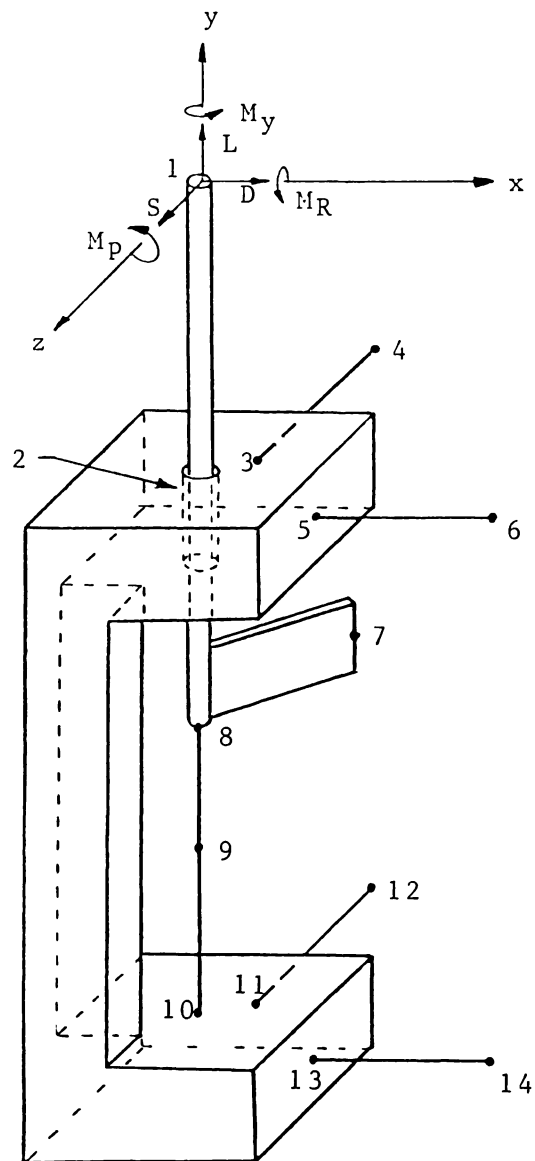


Fig. 45. Six component floating beam hardware tolerance locations.

Example D: Three component pyramidal balance

1. From the static analysis, the measured reactions were found to be:

$$P = M_p/k$$

$$R_D = -D$$

$$R_L = L$$

2. Therefore,

P : function of 1 applied load

R_D : " 1 "

R_L ; " 1 "

--> $c = 3$

3. For the three measured reactions: $n = c/3$

==> $n = 1$

This result ($n = 1$) simply indicates that the balance is uncoupled. Furthermore, one is the minimum degree of coupling that can be attained.

4. Identify the areas where tolerances are of a concern:

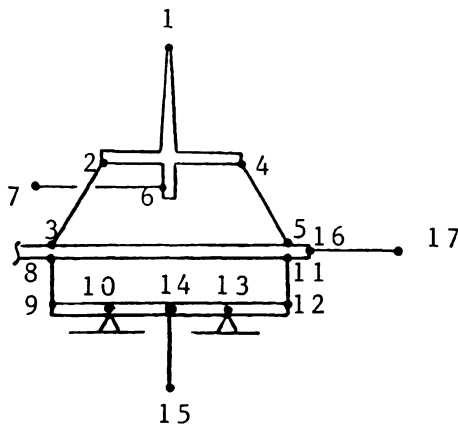


Fig. 46. Three component pyramid hardware tolerance locations.

Now note which areas are affected by each applied load:

Lift: 1, 2, 3, 4, 5, 8, 9, 10, 11, 12, 13, 14, 15

--> 13 areas affected

Drag: 1, 2, 3, 4, 5, 8, 9, 10, 11, 12, 13, 14, 16, 17

--> 14 areas affected

M_p : 1, 2, 3, 4, 5, 6, 7, 8, 9, 10, 11, 12, 13, 14

--> 14 areas affected

Thus, $s = 13 + 14 + 14 = 41$

Since this is a three component balance, the hardware parameter is: $p = s/3$

$$\underline{p = 13.7}$$

Example E: Six component pyramidal balance

1. From the static analysis, it was seen that all of the measured reactions are uncoupled. Therefore, it can be stated directly that the degree of coupling is:

3. $\underline{n = 1}$

4. Identify the concerned areas of tolerance from Figure 47 on the next page.

Thus, each individual load path affects:

Lift: 1, 2, 3, 4, 5, 6, 7, 8, 9, 26, 27, 28, 29, 30, 31,
32, 33, 34, 35, 36, 37, 38, 39

--> 23 areas affected

Drag: 1, 2, 3, 4, 5, 6, 7, 8, 9, 20, 21, 22, 23, 24, 25,
26, 27, 28, 29, 30, 31, 32, 33, 34, 35, 36, 37

--> 27 areas affected

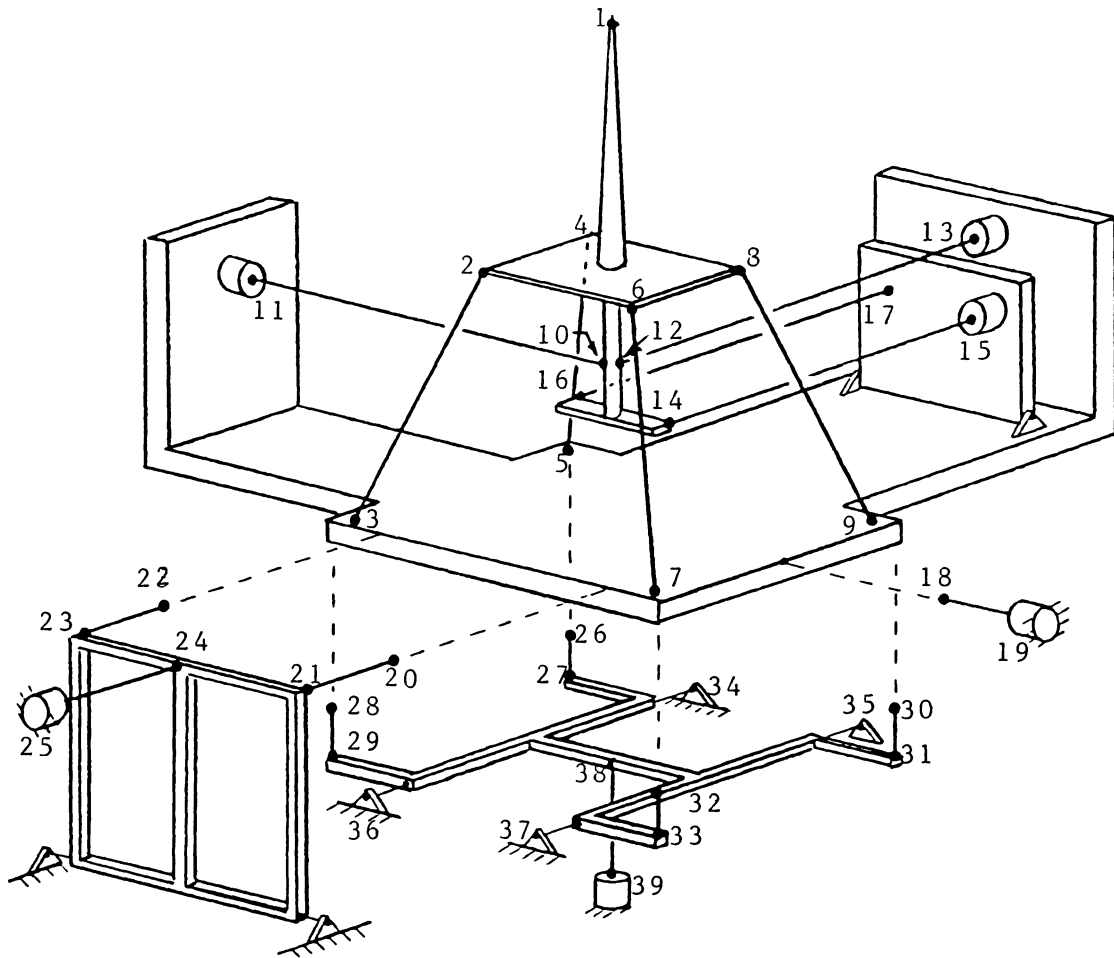


Fig. 47. Six component pyramid hardware tolerance locations.

Side: 1, 2, 3, 4, 5, 6, 7, 8, 9, 18, 19, 26, 27, 28, 29,
30, 31, 32, 33, 34, 35, 36, 37, 38

--> 24 areas affected

Pitch: 1, 2, 3, 4, 5, 6, 7, 8, 9, 12, 13, 26, 27, 28, 29,
30, 31, 32, 33, 34, 35, 36, 37

--> 23 areas affected

Yaw: 1, 14, 15, 16, 17, 20, 21, 22, 23

--> 9 areas affected

Roll: 1, 2, 3, 4, 5, 6, 7, 8, 9, 10, 11, 26, 27, 28, 29,
30, 31, 32, 33, 34, 35, 36, 37, 38

--> 24 areas affected

Therefore, the total areas affected by all of the load
paths:

$$s = 23 + 27 + 24 + 23 + 9 + 24 = 130$$

For a six component balance,

$$p = s/6$$

$$p = \underline{21.7}$$

Example F: Three component smoke tunnel balance

The following design is for measuring the light loads at low Reynolds numbers in the Embry-Riddle smoke tunnel.

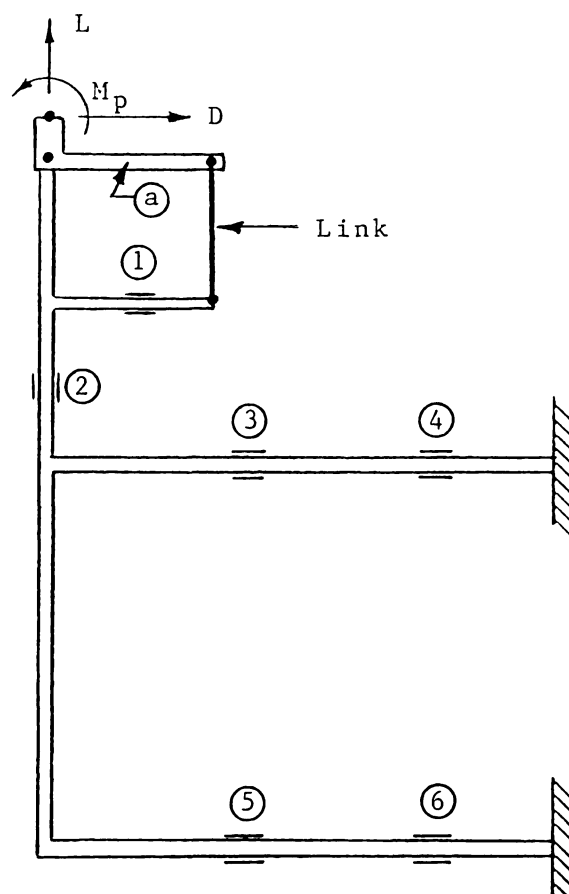


Fig. 48. Three component smoke tunnel balance configuration.

1. For the above configuration, the measured reactions are the bending moments at locations (1) through (6). As discussed in the floating beam example, the axial force effects on the strain gages can be canceled by using a Wheatstone bridge.

For this example, a slightly easier approach will be taken for step 1. Instead of solving for the measured

reactions in detail (which would require the solution of the differential equation for beam deflections), the bending moments will be determined as "functions" of the applied loads by engineering logic.

Observing lever (a), the reaction in the link is clearly a function of D and M_p . Thus, the bending moment at location (1) is also a function of D and M_p :

$$M_1 = f(D, M_p)$$

Likewise, the bending moment at location (2) is also a function of:

$$M_2 = f(D, M_p)$$

For the moments at locations 3, 4, 5, and 6, consider the system deflections:

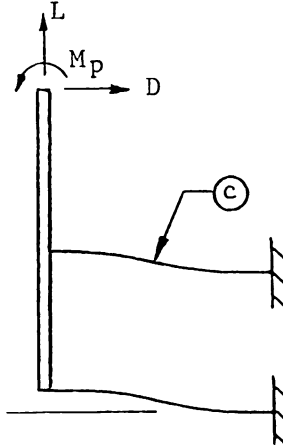


Fig. 49. Smoke tunnel balance deflections.

A free body diagram of element (c) would appear as:

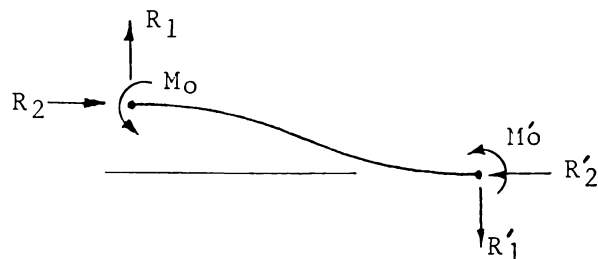


Fig. 50. Free body diagram of smoke tunnel balance element c.

Therefore, for the loads applied to element (c):

$$R_1 = f(L)$$

$$R_2 = f(D, M_p)$$

$$M_o = f(L)$$

Thus, the bending moments along element (c) at locations 3 and 4 are functions of:

$$M_3 = f(L, D, M_p)$$

$$M_4 = f(L, D, M_p)$$

Likewise,

$$M_5 = f(L, D, M_p)$$

$$M_6 = f(L, D, M_p)$$

2. The coupling number, c, is:

$M_1 =$ function of 2 applied loads

$M_2 =$ " 2 "

$M_3 =$ " 3 "

$M_4 =$ " 3 "

$M_5 =$ " 3 "

$M_6 =$ " 3 "

--> c = 16

3. For six measured reactions, the degree of coupling is:

$$n = c/6$$

$$n = \underline{2.667}$$

4. The areas affected for the hardware parameter are:

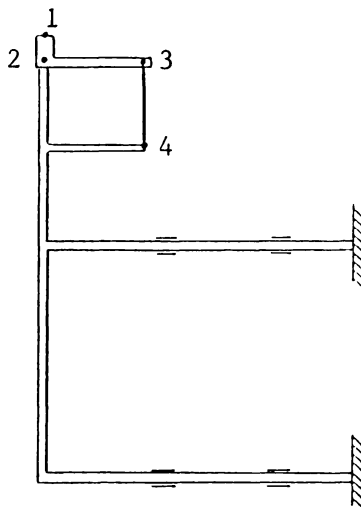


Fig. 51. Smoke tunnel balance hardware tolerance locations.

Therefore,

$$L: 1, 2$$

--> 2 areas affected

$$D: 1, 2, 3, 4$$

--> 4 areas affected

$$M_p: 1, 2, 3, 4$$

--> 4 areas affected

$$\Rightarrow s = 2 + 4 + 4 = 10$$

For a three component balance, the hardware parameter is:

$$p = s/3$$

$$p = \underline{3.333}$$

Example G: Six component platform

The diagram of this balance appears in Figure 52:

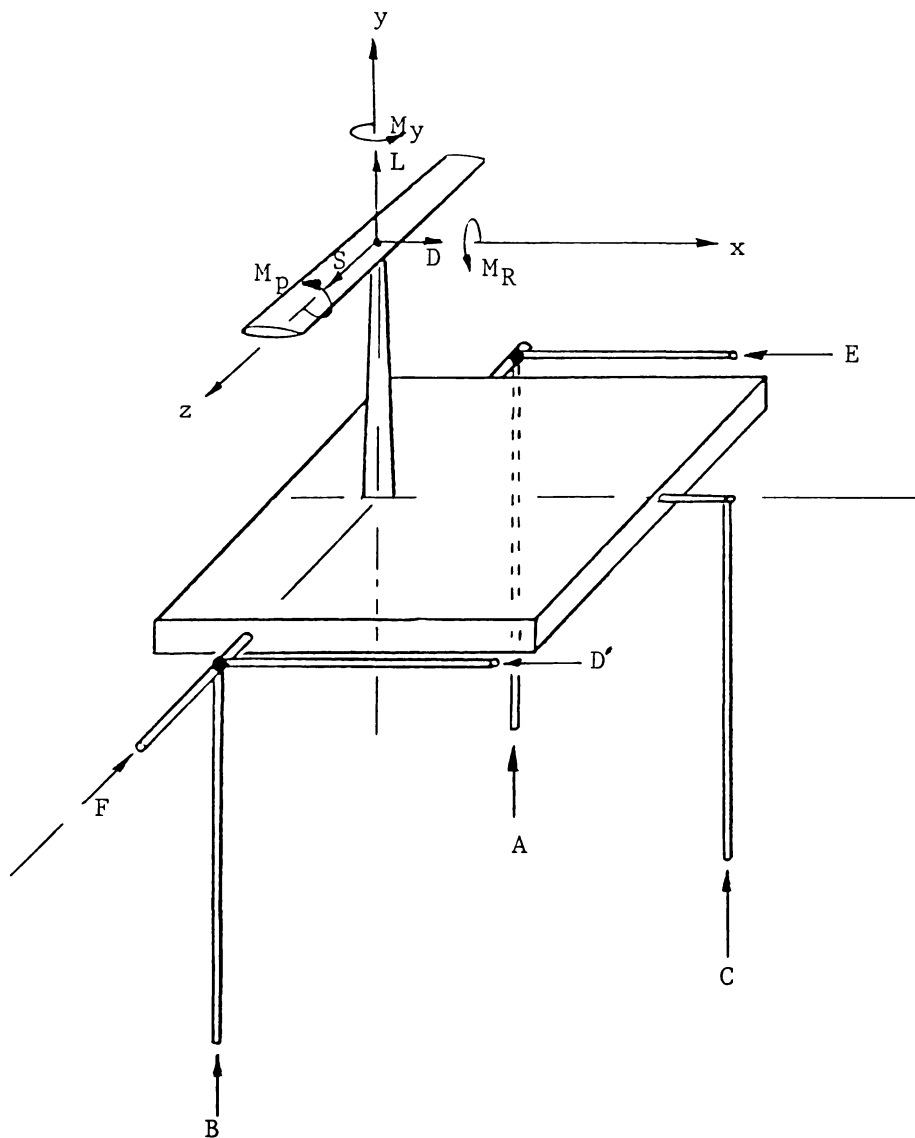


Fig. 52. Six component platform configuration.

1. The measured reactions A, B, C, D', E, and F, as functions of the applied loads, are found by statics to be:

$$A = f(L, D, S, M_R, M_P)$$

$$B = f(L, D, S, M_R, M_P)$$

$$C = f(D, M_P)$$

$$D' = f(D, M_Y)$$

$$E = f(D, M_Y)$$

$$F = f(S)$$

2. The coupling number, c , is found to be:

A: function of 5 applied loads

B: " 5 "

C: " 2 "

D': " 2 "

E: " 2 "

F: " 1 "

--> $c = 17$

3. For six measured reactions:

$$n \equiv \underline{2,833}$$

4. Figure 53 shows the areas where tolerances are of concern. The areas affected by each load are:

L: 1, 2, 4, 6, 8, 9, 10

--> 7 areas affected

D: 1, 2, 4, 5, 6, 7, 8, 9, 10

--> 9 areas affected

S: 1, 2, 3, 4, 6, 8

--> 6 areas affected

M_p : 1, 2, 4, 6, 8, 9, 10

--> 7 areas affected

M_R : 1, 2, 4, 6, 8

--> 5 areas affected

M_Y : 1, 2, 4, 5, 7

--> 5 areas affected

==> $s = 39$

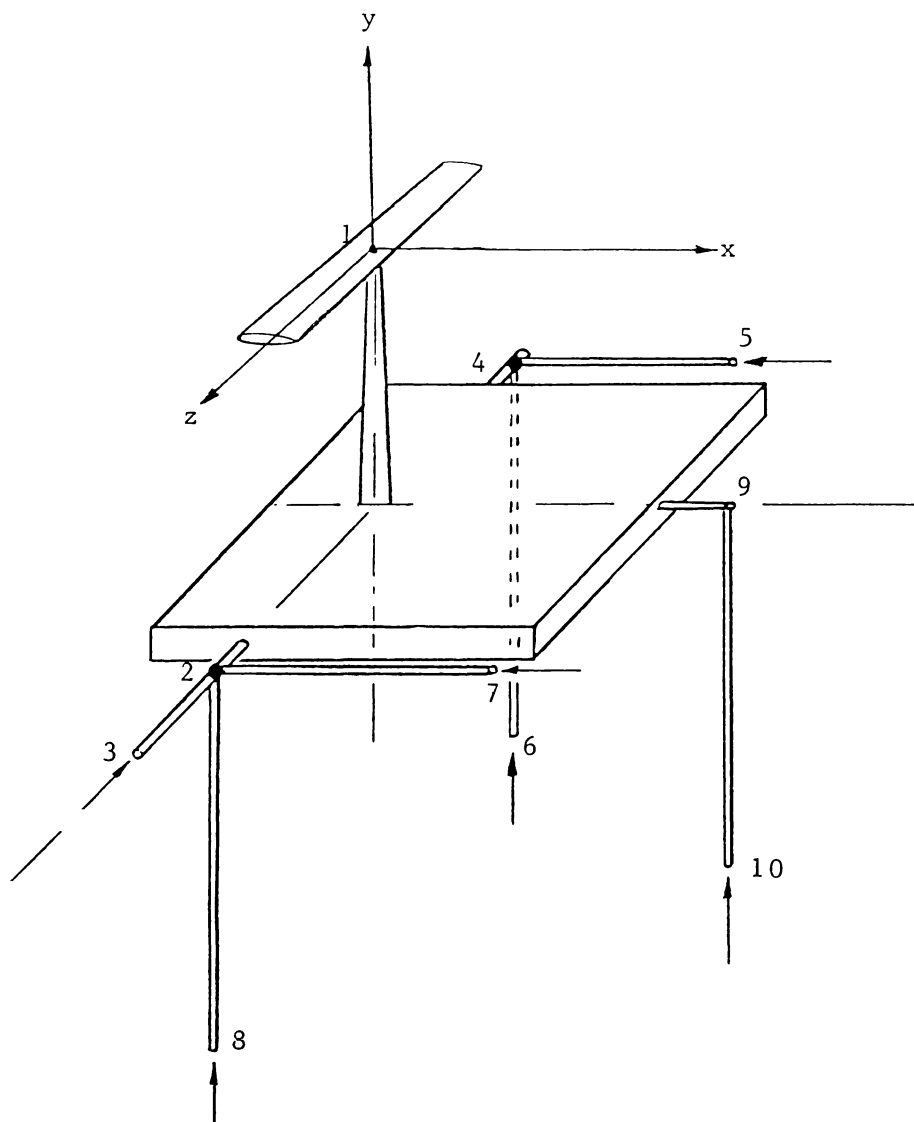


Fig. 53. Platform balance hardware tolerance locations.

For a six component balance, the hardware parameter is:

$$p = s/6$$

$$p \cong \underline{6.5}$$

Example H: Six component yoke balance

This balance is configured as in Figure 54:

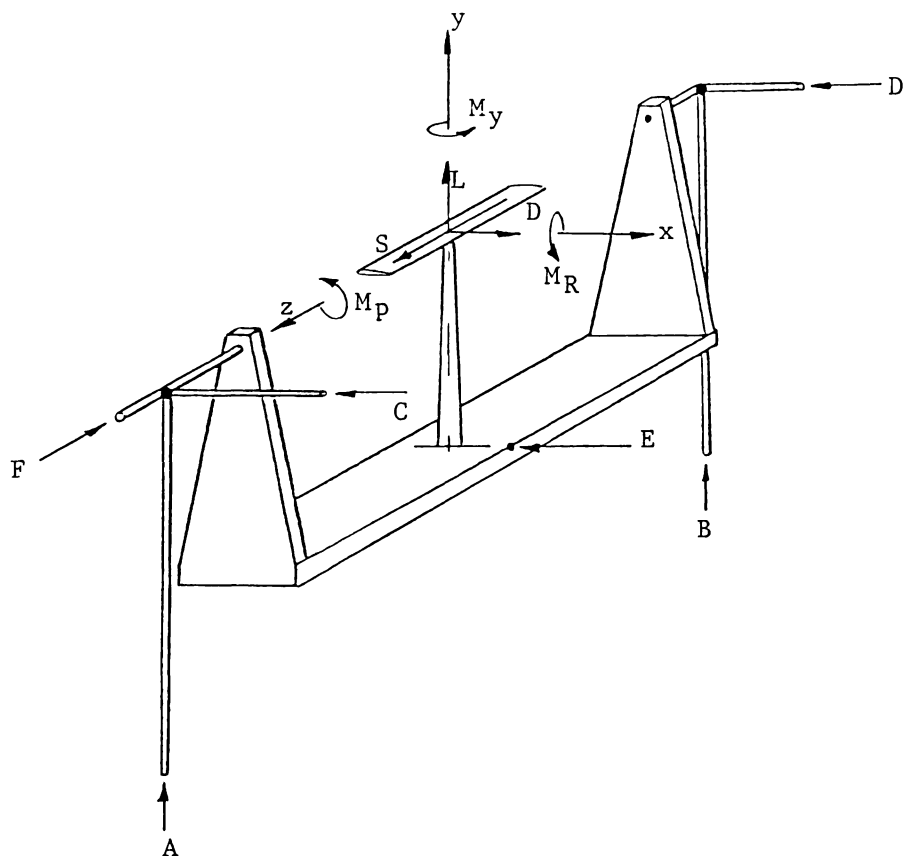


Fig. 54. Six component yoke configuration.

1. The measured reactions A, B, C, D', E, and F are found to be functions of the following loads:

$$A: = f(L, M_R)$$

$$B: = f(L, M_R)$$

$$C: = f(D, M_Y, M_P)$$

$$D': = f(D, M_Y, M_P)$$

$$E: = f(M_P)$$

$$F: = f(S)$$

2. A = function of 2 applied loads
 B = " 2 "
 C = " 3 "
 D' = " 3 "
 E = " 1 "
 F = " 1 "

--> c = 12

3. Therefore, for six measured reactions:

$$\underline{n = 2}$$

4. The areas of concern for hardware tolerances are:

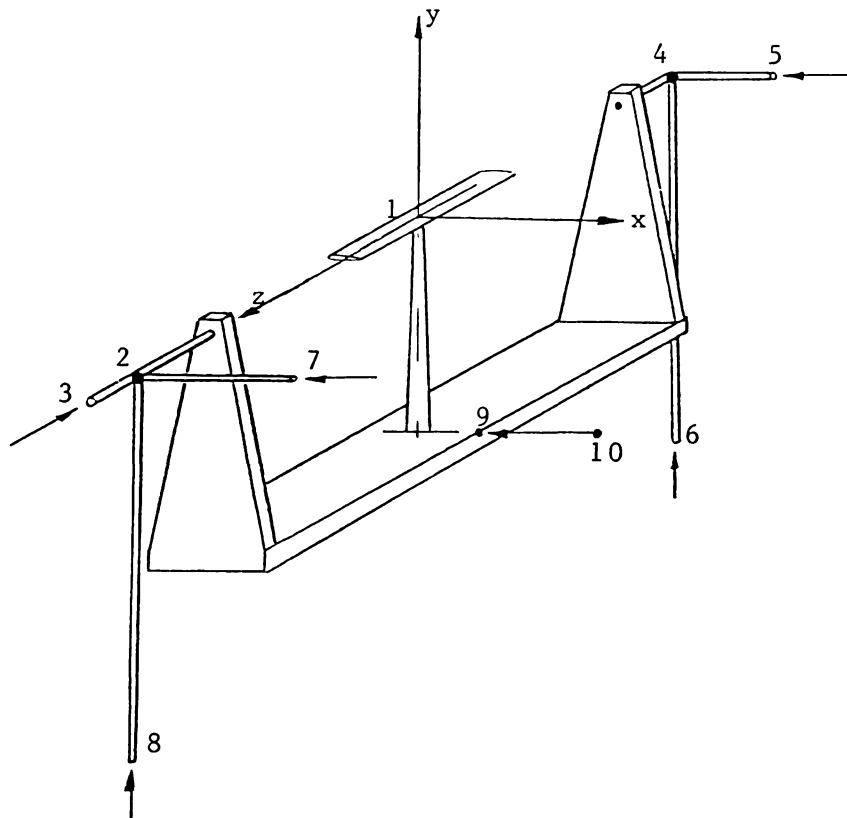


Fig. 55. Yoke balance hardware tolerance locations.

L: 1, 2, 4, 6, 8

--> 5 areas affected

D: 1, 2, 4, 5, 7

--> 5 areas affected

S: 1, 3

--> 2 areas affected

M_R: 1, 2, 4, 6, 8

--> 5 areas affected

M_Y: 1, 2, 4, 5, 7

--> 5 areas affected

M_P: 1, 2, 4, 5, 7, 9, 10

--> 7 areas affected

Therefore: $s = 29$

For a six component balance,

$$p = s/6$$

$$p = \underline{4.83}$$

BIBLIOGRAPHY

1. Anderson, John D. Introduction to Flight. New York: McGraw-Hill, Inc., 1978.
2. Josephy, Alvin M., ed. The American Heritage History of Flight. American Heritage Publishing Co., 1962.
3. Randers-Pehrson, N. H. Pioneer Wind Tunnels. Washington: Smithsonian Institution, 19 January, 1935.
4. McFarland, Marvin W., ed. The Papers of Wilbur and Orville Wright. New York: McGraw-Hill, Inc., 1953.
5. Gorlin, S. M. Wind Tunnels and Their Instrumentation. Jerusalem: Israel Program for Scientific Translations, 1966.
6. Pope, Alan. Low Speed Wind Tunnel Testing. New York: John Wiley and Sons, 1966.
7. Kerneis, Jean. Wire Suspensions In Wind Tunnel Experiments. Washington, D.C.: National Advisory Committee for Aeronautics (NACA), 1925. TM 342.
8. Norton, F. H. Design of Recording Wind Tunnel Balances. Langley Field, Va.: National Advisory Committee for Aeronautics (NACA), 1920. TM 30.
9. Phillips, Edward H. "Magnetic Suspension Studied for Large Scale Wind Tunnel." Aviation Week and Space Technology, 11 April 1988, 41.
10. Holman, J. P. Experimental Methods for Engineers. New York: McGraw-Hill, Inc., 1984.
11. Weber, P. J. Some Investigations of the Limits of the Working Range of Metallic Spring Materials for Wind-Tunnel Balances with Strain-Gauge Systems. European Space Research Organization, 1973.